Synthesis, evaluation and mechanistic insights of novel IMPDH inhibitors targeting ESKAPEE bacteria

Nour Ayoub, Amit Upadhyay, Arnaud Tête, Nicolas Pietrancosta, Hélène Munier-Lehmann, Timothy O'Sullivan

European Journal of Medicinal Chemistry 280 (2024) 116920

Contents lists available at ScienceDirect

European Journal of Medicinal Chemistry

journal homepage: www.elsevier.com/locate/ejmech

Research paper

Synthesis, evaluation and mechanistic insights of novel IMPDH inhibitors targeting ESKAPEE bacteria

Nour Ayoub [a,2], Amit Upadhyay [b,c,d,2], Arnaud Tête [e], Nicolas Pietrancosta [f,g], Hélène Munier-Lehmann [a,1,**], Timothy P. O'Sullivan [b,c,d,*,1]

[a] Université Paris Cité, INSERM UMRS-1124, Institut Pasteur, Structural Biology and Chemistry Department, F-75006, Paris, France
[b] School of Chemistry, University College Cork, Cork, Ireland
[c] School of Pharmacy, University College Cork, Cork, Ireland
[d] Analytical and Biological Chemistry Research Facility, University College Cork, Cork, Ireland
[e] Université Paris Cité, INSERM UMRS-1124, F-75006, Paris, France
[f] Sorbonne Université, École Normale Supérieure, PSL University, CNRS, Laboratoire des Biomolécules, LBM, F-75005, Paris, France
[g] Sorbonne Université, INSERM, CNRS, Neuroscience Paris Seine - Institut de Biologie Paris Seine (NPS - IBPS), F-75005, Paris, France

ARTICLE INFO

Keywords:
Nucleotide metabolism
IMPDH
Inhibitors
Antibacterials
ESKAPEE bacteria
Heteroaryls

ABSTRACT

Antimicrobial resistance poses a significant threat to global health, necessitating the development of novel therapeutic agents with unique mechanisms of action. Inosine 5′-monophosphate dehydrogenase (IMPDH), an essential enzyme in guanine nucleotide biosynthesis, is a promising target for the discovery of new antimicrobial agents. High-throughput screening studies have previously identified several urea-based leads as potential inhibitors, although many of these are characterised by reduced chemical stability. In this work, we describe the design and synthesis of a series of heteroaryl-susbtituted analogues and the evaluation of their inhibitory potency against IMPDHs. Our screening targets ESKAPEE pathogens, including *Pseudomonas aeruginosa*, *Staphylococcus aureus* and *Escherichia coli*. Several analogues with submicromolar inhibitory potency are identified and show no inhibitory potency on human IMPDH nor cytotoxic effects on human cells. Kinetic studies revealed that these molecules act as noncompetitive inhibitors with respect to the substrates and ligand virtual docking simulations provided insights into the binding interactions at the interface of the NAD^+ and IMP binding sites on IMPDH.

1. Introduction

Antimicrobial resistance (AMR) is the evolutionary process by which microbes, such as bacteria, fungi and parasites, become insensitive to the effects of medical treatments. The impact of AMR on human health is significant - in 2019 alone, the number of deaths associated with AMR was estimated to be 4.95 million [1]. Worryingly, this number is expected to rise sharply into the future and could reach 10 million by 2050 based on current trajectories [2]. Increased consumption and inappropriate prescribing of antibiotics has been further exacerbated since the outbreak of the COVID-19 pandemic [3,4]. At the same time, few new classes of antibiotics have come to market [5]. There is also growing concern about reports of resistance to both newer generation antibiotics and antimicrobials of last resort [6–8]. Faced with this growing threat, there is an urgent need for the development of drugs with novel modes of action [9].

One target attracting greater attention over recent years is inosine 5′-monophosphate dehydrogenase (IMPDH), which is an important enzyme for the biosynthesis of nucleotides [10,11]. Inosine-5′-monophosphate (IMP) is a product of the *de novo* purine biosynthesis pathway and is a common precursor to guanine and adenine nucleotides [12]. IMP is converted into xanthosine-5′-monophosphate (XMP) by the action of IMPDH, with NAD^+ as a cofactor being reduced to NADH in the process [13]. This represents the rate-limiting step in the biosynthesis of guanine nucleotides. XMP is further converted to guanosine monophosphate (GMP) through a process catalysed by GMP

* Corresponding author. School of Chemistry, University College Cork, Cork, Ireland.
** Corresponding author. Université Paris Cité, Institut Pasteur, Structural Biology and Chemistry Department, Paris, France.
E-mail addresses: helene.munier-lehmann@pasteur.fr (H. Munier-Lehmann), tim.osullivan@ucc.ie (T.P. O'Sullivan).
[1] These authors contributed equally.
[2] These authors contributed equally.

https://doi.org/10.1016/j.ejmech.2024.116920
Received 11 August 2024; Received in revised form 17 September 2024; Accepted 25 September 2024
Available online 27 September 2024

synthase. Ultimately, GMP is transformed into the building blocks of DNA (i.e. 2′-deoxyguanosine-5′-triphosphate dGTP) and RNA (i.e. guanosine-5′-triphosphate GTP). Inhibition of IMPDH results in the reduction of the guanine pool and, more importantly, in the imbalance between guanine and adenine pools, which is essential for rapidly proliferating cells. Unsurprisingly, IMPDH inhibitors have been extensively studied as putative anti-cancer agents, although none has yet achieved clinical approval [14]. Mycophenolic acid is employed clinically as an immunosuppressant to prevent rejection of transplanted organs and in the treatment of autoimmune diseases such as lupus and Crohn's [10,15,16]. Moreover, it has been demonstrated that the *guaB* gene (encoding IMPDH) is essential for many bacterial pathogens, particularly under infection conditions [10]. Bacterial IMPDHs are, therefore, promising targets for the development of new antibiotics, even though they have been less explored to date. Although eukaryotic and prokaryotic IMPDH catalyse the same chemical transformations, they are marked by different biochemical and structural properties [10, 17–19]. Studies have shown that the IMP binding site and the nicotinamide subsite of the cofactor site are highly conserved. By contrast, the adenosine and pyrophosphate binding regions of the cofactor binding site have strongly diverged [20]. These variations facilitate the design of selective IMPDH inhibitors.

Hedstrom and colleagues have successfully developed a series of oxime-containing urea-based inhibitors which were confirmed to be highly potent inhibitors of microbial IMPDH [21]. For example, an I_{50} of 0.66 nM was recorded for oxime **1** against *Cryptosporidium parvum* IMPDH while **2** was found to inhibit *Bacillus anthracis* IMPDH with an I_{50} of 2 nM (Fig. 1) [22]. However, one inherent drawback of this series is the reduced metabolic stability of the oxime functional group. We wondered whether substitution of the oxime by a bioisosteric equivalent would constitute a fruitful research avenue. There exists literature precedent for this approach. Newhouse and co-workers have previously demonstrated how replacement of an oxime in a B-Raf kinase led to a pyrazole-based inhibitor that retained biological activity [23]. Jung has similarly shown how incorporation of a 1,2,3-triazole in place of an oxime produced a series of potent mitochondrial permeability transition pore blockers with increased cytochrome P450 stability [24]. Exchanging the oxime in **1** with a suitable aryl or heteroaryl equivalent, such as the pyrazole in **3**, could provide access to effective IMPDH inhibitors. In this paper, we outline our work to date on the synthesis of a library of similar molecules and their subsequent evaluation as inhibitors of bacterial IMPDHs of three antibiotic resistant ESKAPEE pathogens, namely *Pseudomonas aeruginosa*, *Staphylococcus aureus* and *Escherichia coli*. The mode of inhibition has been further characterised by kinetic studies and their potential binding mode has been investigated through ligand virtual docking. This chemical series shows promising inhibitory properties without any effect on human cell viability.

2. Results and discussion

2.1. Chemistry

Access to a library of benzylurea analogues required the initial synthesis of aryl bromide **9** as a common intermediate (Fig. 2). Starting from 2-(3-bromophenyl)acetic acid (**5**), ethyl ester **6** was prepared in near quantitative yield by the addition of thionyl chloride to carboxylic acid **5** in ethanol [25]. Double α-alkylation of ester **6** with sodium hydride and methyl iodide afforded *gem*-dimethyl **7** which was subsequently hydrolysed to carboxylic acid **8**. Installation of the urea group was achieved by treatment of **8** with ethyl chloroformate and sodium azide to generate the corresponding carboxylic azide which underwent Curtius rearrangement on heating to the isocyanate. The isocyanate was not isolated but instead treated with benzylamine to furnish benzylurea **9** in an overall yield of 45 %. Evidence for the formation of the urea was found in the ^{1}H NMR spectrum of **9** with the urea protons appearing as a 1H triplet at 4.60 ppm and a 1H singlet at 4.96 ppm, in addition to a 2H doublet at 4.22 ppm for the benzylic protons.

Although aryl bromide **9** could be potentially directly coupled to various boronic acids or esters, Suzuki-Miyaura reactions involving heteroaromatic rings are often more challenging. For that reason, we adopted a coupling methodology previously reported by Fu et al. which was optimized for nitrogen heterocycles [26]. Our modified coupling procedure employed 1 mol% tris(dibenzylideneacetone)dipalladium as the catalyst and 1.7 equivalents of tripotassium phosphate as a base in dioxane/water (10:1). Whereas Fu obtained good yields with tricyclohexylphosphine, its use as ligand in this case resulted in significant amounts of unreacted starting material. Switching to 2 mol% triphenylphosphine under microwave heating at 100 °C for 1.5 h improved conversions and decreased overall reaction times. These couplings were generally low yielding (Table 1, entries 1–5) with incomplete consumption of starting material still observed, likely due to interference from the urea functional group with the catalytic cycle. Yields ranging from 10 % for the furan analogue (entry 3) to 50 % for the thiophene derivative (entry 4) were recorded. A simple phenyl derivative (entry 5) was also prepared to determine whether the incorporation of a heteroaryl group at the 2-position was a prerequisite for biological activity.

We next incorporated a 3-nitro-4-chlorophenyl ring as this substitution pattern had been previously associated with good IMPDH inhibition [21]. Given the difficulties experienced with our initial late-stage coupling approach, the synthetic plan was revised to place the coupling step at the start of the synthesis. Employing conditions developed by Schneider et al., heteroaryl boronate esters or acids were coupled to aryl bromide **7** using a combination of palladium tetrakis and sodium carbonate under microwave heating (Table 2, entries 1–5) [27]. Unlike the late-stage couplings, full consumption of starting material was observed in all cases with much improved yields ranging from 60 % for the 4-pyrazole derivative (entry 1) to 95 % for the 3-pyrazole analogue (entry 2). Given that 2-halosubstituted pyridines readily undergo aromatic substitution reactions, 2-fluoropyridine derivative **20** was also prepared to investigate its use as an irreversible inhibitor. As certain heteroaryl boronates were not readily accessible, the corresponding heteroaryl bromides were instead coupled to known boronate ester **15** (entries 6–8) [25]. An attempted coupling of aryl boronate ester **15** with bromoimidazole derivatives was not successful necessitating prior protection of the NH group. The *N*-alkylated aryl esters were obtained in moderate yields of 45 % for 4-imidazole **22** (entry 7) and 44 % for 2-imidazole **23** (entry 8).

The individual ethyl esters were next hydrolysed using five

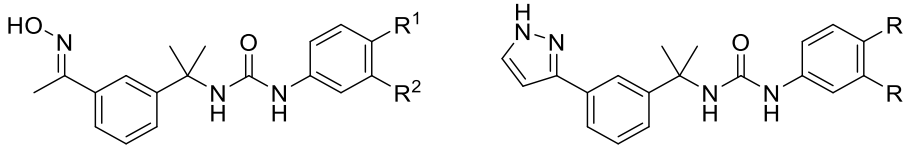

1 : R^1 = Cl, R^2 = NO_2
2 : R^1 = Cl, R^2 = CF_3

3

Fig. 1. Comparison of oxime-vs heteroaryl-containing IMPDH inhibitors.

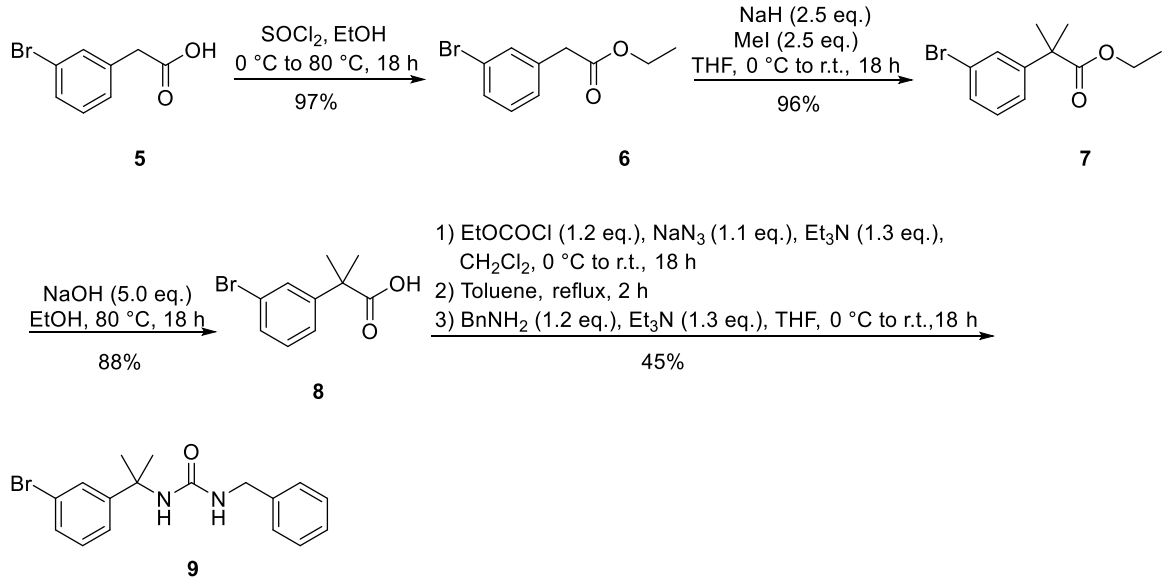

Fig. 2. Synthetic route to aryl bromide **9**.

Table 1
Preparation of benzylurea analogues via late-stage Suzuki-Miyaura coupling.

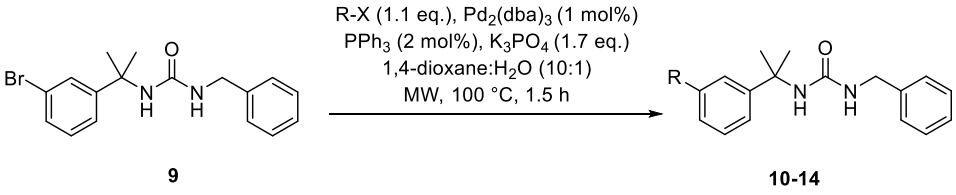

Entry	R	X	Urea	Yield
1.	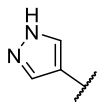	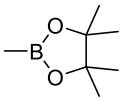	**10**	15 %
2.	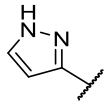	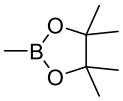	**11**	17 %
3.		-B(OH)$_2$	**12**	10 %
4.		-B(OH)$_2$	**13**	50 %
5.	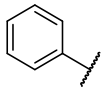	-B(OH)$_2$	**14**	20 %

equivalents of sodium hydroxide in ethanol heated to 80 °C (Table 3). The resulting carboxylic acids were mostly isolated as solids following work up in yields ranging from 40 % (entry 7) to 98 % (entry 1). Attempted hydrolysis of 2-fluropyridine-containing ester **20** in this manner did not proceed as planned but unexpectedly afforded 2-ethoxypyridine-substituted carboxylic acid **31** in 86 % yield (entry 8). Substitution of the fluorine with an ethoxy group was confirmed by ^{19}F NMR analysis as well as the absence of ^{19}F–^{13}C coupling in the ^{13}C NMR spectrum. The desired 2-fluropyridine derivative **32** was instead obtained in 58 % yield by heating **20** in an aqueous solution of sodium hydroxide in refluxing DMF (entry 9) [28]. Each of the carboxylic acids **24**–**32** was subjected to the previously described protocol for the

Table 2
Early-stage Suzuki-Miyaura couplings.

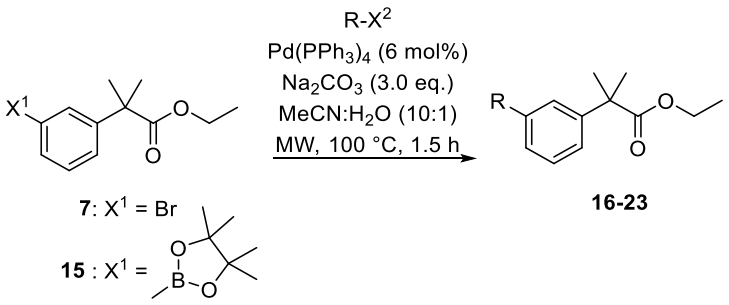

Entry	Starting material	X^1	R	X^2	Ester	Yield
1.	**7**	Br	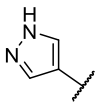	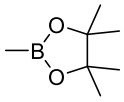	**16**	60 %
2.	**7**	Br	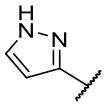	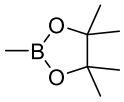	**17**	95 %
3.	**7**	Br		$-B(OH)_2$	**18**	84 %
4.	**7**	Br		$-B(OH)_2$	**19**	79 %
5.	**7**	Br	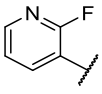	$B(OH)_2$	**20**	94 %
6.	**15**	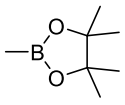	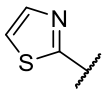	Br	**21**	92 %
7.	**15**	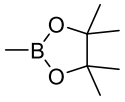	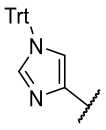	Br	**22**	45 %
8.	**15**	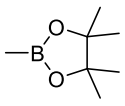	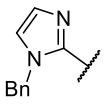	Br	**23**	44 %

installation of the urea group i.e. conversion of the carboxylic acid, subsequent rearrangement to the isocyanate, followed by addition of 3-nitro-4-chloroaniline. Evidence for the successful transformation was found in the ^{1}H NMR spectra with the urea protons appearing as singlet peaks at 6.36 ppm and 8.09 ppm respectively in the case of **33**, along with the urea carbonyl at 154.2 ppm in the ^{13}C NMR spectrum. Acylation of pyrazoles **24** and **25** was observed during their conversion into corresponding ureas **33** and **34**. The yields for these steps were moderate with an average of 28 % recorded for ureas **33**–**41** (entries 1–9) which could be attributed to the low recovery of the target molecules during column chromatography arising from co-elution of side products.

Finally, cleavage of the ethoxycarbonyl group from **33** and **34** was achieved following a method reported by Bai and co-workers [29]. Acylated pyrazoles **33** and **34** were stirred in a methanolic solution of triethylamine at room temperature and pyrazoles **42** and **43** were isolated in yields of 66 % and 82 % respectively (Fig. 3). Employing conditions developed by Lee and colleagues, the trityl protecting group in **38** was removed using acetic acid in methanol to produce imidazole **44** in 23 % yield as an off-white solid [30]. Attempted deprotection of **39** was unsuccessful, so the *N*-benzyl derivative was carried forward for biological evaluation.

Table 3
Preparation of 3-nitro-4-chlorophenylureas.

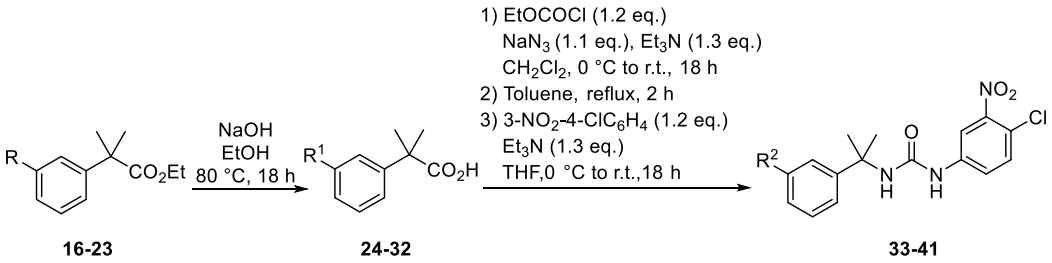

Entry	R^1	Carboxylic acid	Yield	R^2	Urea	Yield
1.	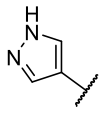	**24**	98 %	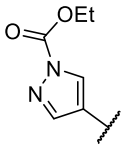	**33**	12 %
2.	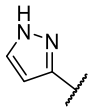	**25**	70 %	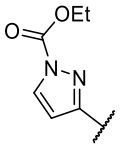	**34**	30 %
3.		**26**	94 %		**35**	25 %
4.		**27**	83 %		**36**	13 %
5.		**28**	78 %		**37**	32 %
6.	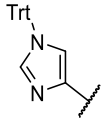	**29**	98 %	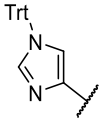	**38**	46 %
7.	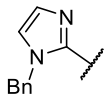	**30**	40 %	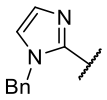	**39**	59 %
8.	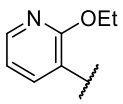	**31**	86 %	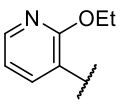	**40**	20 %
9.	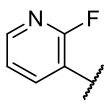	**32**[a]	58 %	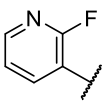	**41**	15 %

[a] NaOH (15 % aq. solution), DMF, 100 °C, 24 h.

2.2. Biochemical evaluation and characterisation

2.2.1. Structure activity relationships on IMPDH from P. aeruginosa (IMPDHpa)

In order to evaluate the inhibitory activity of the newly synthesized compounds, *in vitro* enzymatic assays were performed on IMPDHpa. *P. aeruginosa* is a ubiquitous environmental bacterium notorious for its high virulence and ability to cause a diverse array of healthcare-associated infections, including respiratory tract infections, hospital acquired pneumonia and ventilator-associated pneumoni, kurinary tract infection, blood stream infections, osteomyelitis and endocarditis. Its pathogenicity is further exacerbated by its intrinsic resistance to

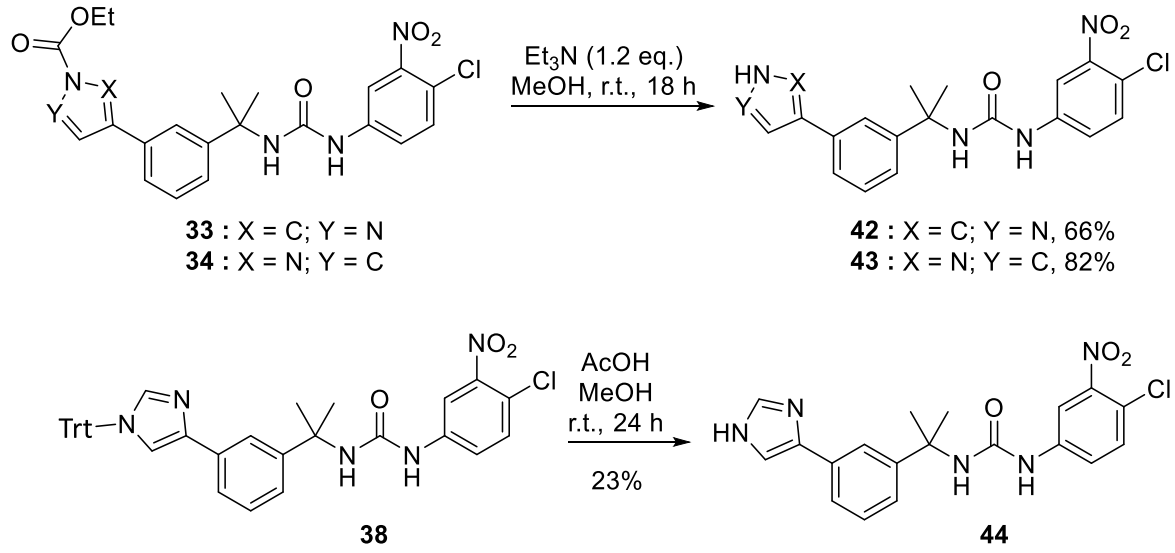

Fig. 3. Deprotection of pyrazoles **33**, **34** and imidazole **38**.

multiple classes of antibiotics, making it a formidable challenge in clinical settings [31]. IMPDHpa was overexpressed in *E. coli* and purified in a two-step procedure for the evaluation of the urea derivatives (see Experimental section) [32]. The assays monitored the production of NADH at 340 nm under non-saturating substrate conditions, specifically using 0.2 mM IMP and 0.4 mM NAD^+, in the presence of 0.2 mM MgATP and 2 mM $MgCl_2$ [26]. The activity measured in the absence of any compound was taken as 100 % of catalytic activity. Each compound was tested at 50 μM concentration and the corresponding percentage inhibition was calculated (Fig. 4A and Table 4).

The compounds ranged in efficacy from 99 % inhibition for 3-nitro-4-chlorophenyl-substituted 3-pyrazole **43** (Table 4, entry 16) to 10 % for furan-containing benzylurea **12** (entry 3). As illustrated by Fig. 4A, a clear trend emerged where all the benzylureas **10**–**14** (entries 1 to 5) were considerably less potent (median value of enzyme inhibition = 15 %) than the corresponding 3-nitro-4-chlorophenyl derivatives **33**–**44** (median value of enzyme inhibition = 96 %) (entries 6 to 17). This trend suggests that the 3-nitro-4-chlorophenyl substituent is important for effective inhibition of IMPDHpa. This result is not especially surprising, as a 3,4-disubstitution pattern is strongly associated with increased inhibitory activity of IMPDH enzymes, with the 3-nitro-4-chlorophenyl motif ranking among the more favorable in both *in vitro* and *in vivo* studies [21,34,35].

Within the 3-nitro-4-chlorophenyl series, trityl-protected 4-imidazole derivative **38** (entry 11) was much less effective than non-

Table 4
Inhibition of IMPDHpa catalytic activity. The % of inhibition was established for each compound at 50 μM. For those with >80 % inhibition, I_{50} values have been determined as described in the Experimental section. Positive control **M18** [33]: 90 % inhibition at 57 μM and I_{50} = 3.62 ± 0.44 μM.

Entry	Urea	% inhibition at 50 μM	I_{50} (μM)
1.	**10**	29 ± 7	ND
2.	**11**	59 ± 5	ND
3.	**12**	10 ± 9	ND
4.	**13**	15 ± 3	ND
5.	**14**	16 ± 10	ND
6.	**33**	87 ± 2	0.42 ± 0.05
7.	**34**	98 ± 1	0.16 ± 0.04
8.	**35**	96 ± 3	0.14 ± 0.03
9.	**36**	99 ± 1	0.26 ± 0.05
10.	**37**	97 ± 4	0.11 ± 0.02
11.	**38**	35 ± 5	ND
12.	**39**	63 ± 2	ND
13.	**40**	95 ± 3	0.59 ± 0.21
14.	**41**	98 ± 1	0.24 ± 0.02
15.	**42**	97 ± 4	0.13 ± 0.02
16.	**43**	99 ± 2	0.11 ± 0.01
17.	**44**	99 ± 10	0.10 ± 0.02

ND: Not determined.

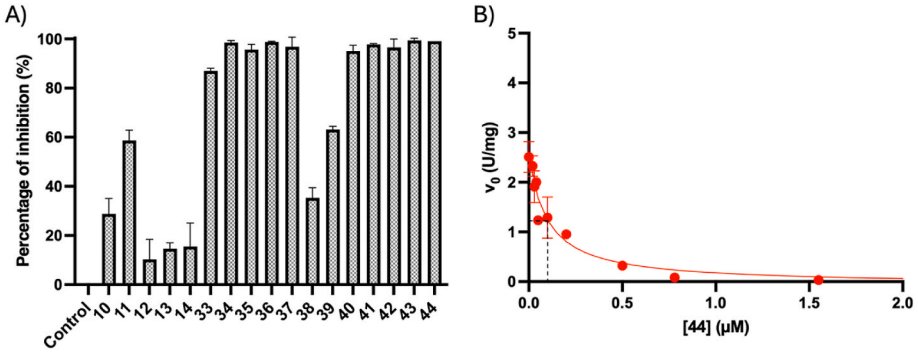

Fig. 4. Evaluation of the synthesized compounds on IMPDHpa catalytic activity. A) Histogram representation of the % inhibition of IMPDHpa in the presence of 50 μM of each compound. B) Dose-response plot of IMPDHpa as a function of variable concentrations of compound **44** as an example to determine its I_{50} value (see dotted lines on the graph).

protected 4-imidazole **44** (entry 17). Similarly, benzyl-protected 2-imidazole derivative **39** (entry 12) displayed relatively poor IMPDHpa inhibition of 63 %. The presence of a bulky group in *N*-alkylated **38** and **39** likely interferes with receptor binding. A similar but smaller effect was observed for 4-pyrazole **42** (entry 15) with 97 % inhibition recorded versus its *N*-acylated derivative **33** (entry 6) with a lower inhibition of 87 %. By contrast, in the case of 3-pyrazole **43** (entry 17), its corresponding *N*-acylated derivative **34** was equipotent (entry 7).

Analogues that displayed greater than 80 % inhibition of IMPDHpa were considered hit molecules and were selected for determination of their half inhibitory concentrations (I_{50}). Accordingly, I_{50} values were determined for ten 3-nitro-4-chlorophenyl-containing molecules (**33**–**37**, **40**–**44**). Following the same conditions used for the primary screening, I_{50} values were determined using dose-dependent response curves (e.g. Fig. 4B) and the results are presented in Table 4. Gratifyingly, all of the selected analogues successfully inhibited IMPDHpa. The I_{50} values ranged from 0.10 μM for the most active compound, 4-imidazole derivative **44** (entry 17), to 0.59 μM for the least active candidate, 2-ethoxypyridine-containing **40** (entry 13). Although a relatively low I_{50} value was also recorded for **33** (entry 6), residual activity of 15 % was observed at 6 μM and 50 μM concentrations. In general, the selected compounds were highly effective and displayed sub-micromolar I_{50} values. These results also compare well with pyrano- [2,3]-pyrimidine **M18** which we previously identified via high-throughput screening of 15,184 compounds as an allosteric inhibitor of IMPDHpa with an $I_{50} = 3.6 \pm 0.5$ μM [33].

Despite the relatively narrow spread of I_{50} values, it was still possible to discern some structure activity relationships. The most obvious difference was between 4-pyrazole **42** (entry 15) which was three times more potent than its *N*-acylated analogue **33** (entry 6). By contrast, the minor difference in inhibitory activity of 3-pyrazole **43** (entry 16) versus its *N*-acylated derivative **34** (entry 7) would suggest that an *N*-acyl group is not necessarily detrimental to potency. Changing the substituent on the rings did impact on efficacy with an I_{50} for 2-fluoropyridine derivative **41** (entry 14) less than half that of the corresponding 2-ethoxypyridine analogue **40** (entry 13). Similarly, replacing the 2-furyl substituent in **36** (entry 9) with a thienyl ring in **35** (entry 8) produced an inhibitor which was twice as effective. The four most active compounds were characterized by the presence of a five membered nitrogen-containing heteroaryl ring i.e. 2-thiazole **37** (entry 10), 4-pyrazole **42** (entry 15), 3-pyrazole **43** (entry 16) or 4-imidazole **44** (entry 17). The latter three candidates with the lowest I_{50} values (entries 15–17) were selected for further studies to elucidate the mechanism of inhibition.

2.2.2. Inhibition studies on wild-type IMPDHs from *E. coli* and *S. aureus*, and on human IMPDH2

To further characterise the inhibitory potency of the three selected molecules (**42**, **43** and **44**), *in vitro* assays were performed on IMPDH from two other bacterial species, namely *E. coli* (IMPDHec) and *S. aureus* (IMPDHsa). *E. coli*, commonly found in the intestine of humans and animals, is usually harmless although some strains can cause infections such as gastroenteritis, septicemia, pneumonia and urinary tract infections [36,37]. *S. aureus* is a common bacteria responsible for various infections, including bacteremia, septic arthritis, pneumonia, gastroenteritis, meningitis, urinary tract infections and skin and soft tissue infections [38]. The methicillin-resistant strain of *S. aureus* (MRSA) is a major cause of mortality with the World Health Organization listing MRSA as a "priority pathogen'' similar to *P. aeruginosa* [39,40]. The two recombinant proteins were expressed and purified as previously described [41,42]. Compounds **42**–**44** were tested on IMPDHec and IMPDHsa under the same conditions as the ones employed for IMPDHpa (see §2.2.1). Consistent with the results obtained for IMPDHpa, kinetic data confirmed that the three compounds were highly potent inhibitors of both enzymes, with each analogue achieving greater than 85 % inhibition at 50 μM (Table 5).

To assess the selectivity of these compounds for bacterial IMPDHs over their human counterparts, we conducted additional experiments targeting human IMPDH isoform 2. The human genome encodes two IMPDH isoforms, type 1 and type 2 (hIMPDH1 and hIMPDH2), which share 84 % sequence identity and exhibit quite similar kinetic properties [43]. Both isoforms are crucial for guanine nucleotide biosynthesis, with hIMPDH2 being the predominant isoform in proliferating cells [44]. We tested the effect of 50 μM of each compound (**12**, **42**–**44**) on the catalytic activity of hIMPDH2. Notably, none of the compounds significantly inhibited hIMPDH2 at this concentration (Fig. S1), demonstrating a high degree of selectivity for bacterial IMPDHs.

Table 5
Inhibitory potency of **42**, **43** and **44** at 50 μM through *in vitro* assays on IMPDHec and IMPDHsa.

Entry	Compound	IMPDHec	IMPDHsa
		% inhibition	% inhibition
1.	**42**	89 ± 4	93 ± 6
2.	**43**	92 ± 1	94 ± 6
3.	**44**	88 ± 3	89 ± 8

Preliminary screening of compounds **12**, **42**–**44** for their inhibitory effects on growth of methicillin-resistant *S. aureus* (ATCC 43300) was conducted at 32 μg/mL (Table 6). The observed trends were in line with those observed in the enzymatic assays, with benzyl-substituted **12** being inactive (entry 1). By contrast, the 3-nitro-4-chlorophenyl-containing heteroaryl analogues **42**–**44** showed promising activity against methicillin-resistant *S. aureus*.

2.2.3. Deciphering the inhibitory mechanism of the three most promising compounds

IMPDH is composed of two structural domains, i.e. the catalytic and the Bateman domains (see Fig. S2) [10]. The likely binding domain of the compounds was first investigated. For this purpose, three selected highly potent compounds **42**–**44**, as well as compound **12** which has a low inhibitory potency on the WT forms, were tested on two IMPDH variants lacking the Bateman domain (IMPDHpa ΔBD and IMPDHec ΔBD) under the same conditions as employed for the corresponding wild-type enzymes. As shown in Fig. 5A and in Table 7, the catalytic activity of the IMPDHpa ΔBD variant was almost completely inhibited by **42**–**44** at 50 μM, whereas compound **12** remains poorly active (6 ± 5 % inhibition). A similar trend was observed with the IMPDHec ΔBD variant (Table 7).

Kinetic assays were next performed on the three wild-type IMPDHs using four different conditions. The first set of conditions (considered as the reference) matches the non-saturating substrate concentrations (i.e. 0.2 mM IMP, 0.4 mM NAD^+, 0.2 mM MgATP and 2 mM $MgCl_2$) employed previously. For the three remaining conditions, the concentration of one component (i.e. either IMP, NAD^+ or ATP) was increased to 2 mM, while the other concentrations were maintained as per the reference conditions. For each variant, enzyme activity was monitored in the absence or in the presence of a fixed inhibitor concentration that afforded approximately 80 % inhibition under the reference conditions. Data obtained for IMPDHpa confirmed that the compounds do not bind to the NAD^+, IMP or MgATP binding sites given that the percentage inhibition of the three compounds was not affected by the increased substrate concentration. As observed with IMPDHpa, the inhibitory

Table 6
Inhibitory activity of **12**, **42**–**44** on *S. aureus* (ATCC 43300) growth at 32 μg/mL.

Entry	Compound	Average	Standard
		inhibition	deviation
1.	**12**	0.49 %	8.3 %
2.	**42**	61.7 %	10.7 %
3.	**43**	79.3 %	0.4 %
4.	**44**	79.3 %	1.9 %

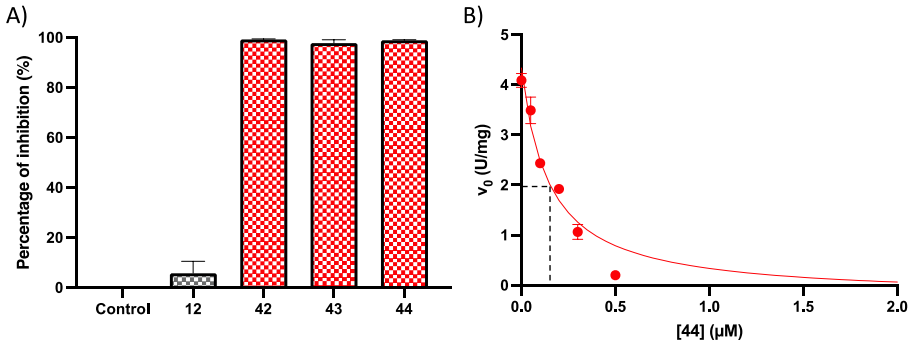

Fig. 5. IMPDHpa ΔBD variant. A) Histogram representation of the % of inhibition of IMPDHpa ΔBD variant in the presence of 50 μM of compound **12** and of the most promising candidates (**42**–**44**; red bars). B) Determination of I_{50} of **44** by dose-response plots of the activity of IMPDHpa ΔBD as a function of variable concentrations of **44**.

Table 7
Inhibitory potency of **12, 42**, **43** and **44** at 50 μM through *in vitro* assays and I_{50} determination on variants lacking the Bateman domain of IMPDHec and IMPDHpa (denoted IMPDHec ΔBD and IMPDHpa ΔBD, respectively).

Entry	Compound	IMPDHec ΔBD		IMPDHpa ΔBD	
		% inhibition	I_{50} (μM)	% inhibition	I_{50} (μM)
1.	**12**	1 ± 3	ND	6 ± 5	ND
2.	**42**	84 ± 1	5.51 ± 1.27	99 ± 1	0.17 ± 0.03
3.	**43**	88 ± 2	4.95 ± 1.10	98 ± 2	0.16 ± 0.04
4.	**44**	90 ± 1	4.26 ± 1.03	99 ± 1	0.15 ± 0.03

ND: Not determined.

effect of the three compounds on IMPDHec and IMPDHsa was not influenced by increased substrate or ATP concentrations. Thus, compounds **42**–**44** are noncompetitive or uncompetitive for both substrates (IMP and NAD^+) and ATP. To further investigate the mode of inhibition of the most active compound (i.e. **44**), we measured the steady-state kinetic parameters of IMPDHpa ΔBD in the absence or in the presence of different concentrations of **44** at a saturating concentration of NAD^+ and variable concentrations of IMP. The experimental data were fitted to the Michaelis-Menten equation (Fig. 6A). Lineweaver-Burk plots were generated to visualize changes in kinetic parameters in the presence of the inhibitor. The results indicate a clear pattern consistent with noncompetitive inhibition (Fig. 6B). These findings further support the conclusion that compounds **42**–**44** are noncompetitive inhibitors that specifically bind to the catalytic domain of IMPDH.

This mode of inhibition prompted us to verify if these compounds are promiscuous inhibitors. We first employed another enzyme (TMP kinase) that has no structural homology and a completely different reaction mechanism compared to IMPDH. TMP kinase from *Mycobacterium tuberculosis* catalyzes the phosphorylation of deoxythymidine 5′-monophosphate (dTMP) to deoxythymidine 5′-diphosphate with MgATP as its preferred phosphoryl donor [45]. The assay was performed as previously described at fixed concentrations of both substrates (dTMP 0.05 mM and MgATP 0.5 mM). Compounds **42**–**44** did not exhibit any inhibitory activity at 20 μM concentration (Fig. S3A).

We also investigated whether the observed inhibition might be a false-positive caused by the sequestration of the protein through colloidal aggregates formation. Accordingly, a detergent-sensitive enzyme-inhibition assay was conducted using Triton X-100 as reported by Feng and Shoichet [46]. The same dose-response assay as depicted in Fig. 5B was performed on IMPDHpa ΔBD under the reference conditions in the presence of 0.01 % Triton X-100, a detergent concentration well tolerated by the enzyme (Fig. S3B). The assay was conducted in the absence and in the presence of various concentrations of **44** to determine the I_{50} value. The results obtained indicated that **44** inhibited the enzyme similarly in both the absence ($I_{50} = 0.15 \pm 0.03$ μM) or in the presence ($I_{50} = 0.14 \pm 0.02$ μM) of detergent. This suggests that **44** does not act as an aggregation-based inhibitor. Taken together, these experiments confirm that the compounds described in this work are specific inhibitors of bacterial IMPDHs.

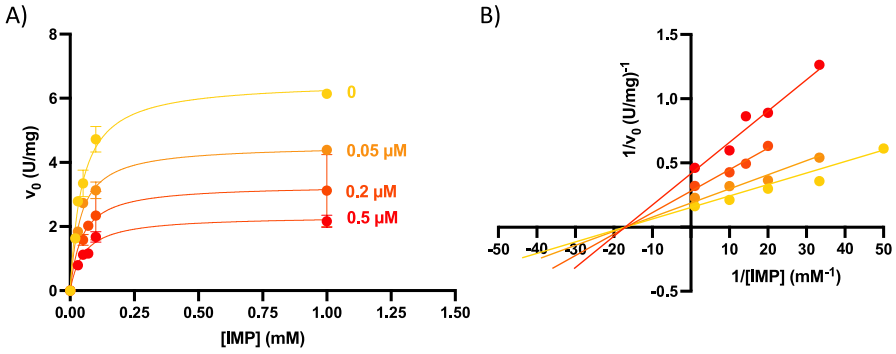

Fig. 6. Steady state kinetics of IMPDHpa ΔBD in the presence of **44**. A) The variation of the initial velocity of IMPDHpa ΔBD as a function of variable concentrations of IMP plotted in the absence (yellow) or in the presence of different concentrations of **44** (orange to red) at saturating concentrations (2 mM) of NAD^+. The tested concentrations of **44** are shown on the right of each curve with a specific color code. B) The inhibition of IMPDHpa ΔBD by compound **44** shown in Lineweaver−Burk representation determined from the variation of the initial velocity of IMPDHpa ΔBD shown in A). The same color code as in A) was used for the different concentrations of **44**.

2.3. Ligand virtual docking

To ensure a complete overview of potential binding sites, we have generated a homology model of IMPDH including unresolved loops based on various templates (pdb: 1ZFJ, 5AHL, 6U8S). Several putative binding sites within the catalytic domain (five main binding pockets) have been identified using a hydrophobic surface profile of IMPDH and Discovery Studio cavity search algorithm. An experimental set of compounds was docked onto each of these cavities. We selected three potent inhibitors (**42**, **43** and **44**) and a poor inhibitor (**12**) of the chemical series described herein, as well as a pyrano- [2,3]-pyrimidine derivative (named **M18**) previously shown to be an allosteric inhibitor binding to the Bateman domain [33]. One site has shown significant binding for **42**, **43** and **44** (Fig. 7). This site is located at the interface between the NAD^+ and IMP binding sites, without competing with these substrates (Fig. 7A). The interacting residues of IMPDHpa with **44** are depicted in Fig. 7B and are highly conserved in the three bacterial IMPDHs selected herein (see sequence alignment, Fig. 7C). Among them, Lys72 is a key residue as it forms a hydrogen bond with the urea moiety, salt bridge with the nitro group and cation-Pi interaction with one aryl moiety of **44** (Fig. 7B). Docking scoring (Fig. 7D) strongly discriminated between **M18** (as expected as this compound binds into the Bateman domain) and, to a lesser extent, **12**, while showing relevant affinity for molecules **42**, **43** and **44**. The common features of the latter is a nitro group enabling one key interaction with Lys72, whereas **12** is devoid of this substitution.

2.3.1. Assessment of cytotoxicity on human cell line and compound stability

To assess potential cytotoxicity of compounds **42**–**44** on human cells, cell viability and cell death were evaluated in human colon Caco-2 cell line after 72h of exposure, by Alamar Blue assay and calculation of the staining ratio of propidium iodide (PI) to Hoechst (H) (PI/H), respectively. Oral administration of drugs, including antibiotics, is often the preferred route of administration [49,50]. Gastrointestinal toxicity is one of the most common adverse effects associated with the use of pharmaceutical agents and is, therefore, a major concern in drug development. The Caco-2 human epithelial cell line is widely used as a model of the intestinal epithelial barrier for cellular toxicity assessment due to their close resemblance to enterocytes [51]. While the positive control 0.2 % of Triton X-100 induced a decrease in cell viability and an increase in cell death, none of the compounds, whether at 1 or 10 μM, had any impact on these parameters (Fig. 8). These results demonstrate that the compounds do not appear to be cytotoxic to human cells. This absence of effect could be attributed to the fact that both human IMPDH isoforms lack the key residue Lys72 (replaced by a histidine), which is involved in the interaction with the nitro group of the most potent compounds such as **44**. This residue may be an important factor influencing the selectivity observed for the chemical series described herein. Finally, **42**–**44** were also tested for their stability in mouse liver microsomes based on a published methodology and demonstrated good stability (>95 % recovery) in both the absence or presence of NADPH after 120 min, comparing favorably to corresponding oxime-based analogues [21,52].

3. Conclusion

In recent years, the IMPDH enzyme has emerged as a promising target for the development of novel antimicrobial agents. This process has been facilitated by high-throughput screens, which have identified several potential leads, such as oximes **1** and **2**. However, the oxime functionality is prone to hydrolysis, prompting a search for more chemically stable alternatives. In this work, we have designed and synthesized a series of heteroaryl-substituted analogues, many of which are effective inhibitors of IMPDHpa. The presence of a 3-nitro-4-chlorophenylurea motif proved important, with the corresponding unsubstituted phenylureas proving significantly less active. Pyrazoles **42**, **43** and imidazole **44** were especially effective with submicromolar activity recorded. Inhibition of IMPDH was not just limited to *P. aeruginosa* but was also true for IMPDH from other ESKAPEE pathogens, including *S. aureus* and *E. coli*. Additional kinetic studies confirmed that these compounds are noncompetitive inhibitors for both the IMP and NAD^+ substrates. Furthermore, **42**–**44** were shown to act on the catalytic domain and not on the Bateman domain. These findings were supported by ligand virtual docking which revealed that the preferred binding pocket lies at the interface of the NAD^+ and IMP binding sites, without directly competing with these substrates Interestingly, the key interacting residue is completely conserved among the bacterial IMPDHs but not in both human counterparts, which might explain the selectivity of this chemical series for the former. These results highlight the potential for further development of this promising chemical series with minimal risk of off-target effects on human IMPDHs.

Competitive inhibitors can lead to adverse side effects due to the similarity of active sites across many enzymes with related functions. For bacterial targets, another issue with such inhibitors is the conservation of active sites in the human counterpart(s), which can lead to poor selectivity and unintended inhibition of human enzymes. The vast majority of the well-known IMPDH inhibitors belongs to this type of inhibitors [10]. In contrast, allosteric inhibitors might offer greater specificity, as allosteric sites are usually more diverse than active sites. This approach has been underexplored for IMPDH. For IMPDHpa, we have previously identified potent allosteric inhibitors which binds into the Bateman domain [33]. However, MgATP is able to displace these compounds. Given the high concentration of MgATP in bacteria, it could be challenging to develop sufficiently potent allosteric compounds that effectively compete for binding. The new chemical series described herein has the advantage of binding to a pocket within the catalytic domain, but without being competitors for the substrates. This binding pocket is not well conserved in humans, and thus selectivity of this chemical series for the bacterial IMPDHs has been demonstrated either on the purified hIMPDH2 and on human cells.

4. Experimental section

4.1. Chemistry

Thionyl chloride, sodium hydride, ethanol, methyl iodide, tetrahydrofuran, methanol, sodium hydroxide, sodium azide, dichloromethane, benzylamine, triphenylphosphine, tripotassium phosphate, phenylboronic acid, sodium carbonate, acetonitrile, acetic acid and ethyl acetate were obtained from Sigma-Aldrich. Triethylamine, tris (dibenzylideneacetone)dipalladium, 2-(3-bromophenyl)acetic acid, palladium chloride, tetrakis(triphenylphosphine)palladium and hexane were obtained from Fluorochem Ltd. Almost all the boronic acids/esters and bromides were also obtained from Fluorochem Ltd. Ethyl chloroformate and toluene were obtained from Thermo Fisher Scientific. 3-Nitro-4-chloroaniline was obtained from TCI Chemicals (Europe). Unless otherwise noted, all the purchased materials and solvents were used without further purification. Compounds were purified by silica gel (Kieselgel 60, 0.040–0.063 mm, Merck) column chromatography. ^1H NMR and ^{13}C NMR spectra were recorded on Bruker Avance 300 (300/75 MHz), Bruker Avance 400 (400/100 MHz), Bruker Avance 500 (500/125 MHz) or Bruker Avance 600 (600/150 MHz) NMR spectrometers respectively. ^{19}F NMR (282/376 MHz) spectra were recorded on Bruker Avance 300/400 NMR spectrometers in proton decoupled mode.

4.1.1. Synthesis of ethyl-2-(3-bromophenyl)acetate (6)[25]

To a stirred solution of 2-(3-bromophenyl)acetic acid (**5**) (5.00 g, 23.251 mmol, 1.0 eq.) in ethanol (50 mL) at 0 °C was added thionyl chloride (7.6 mL) and the reaction mixture was stirred at this temperature for 15 min. The reaction mixture was heated to reflux at 80 °C for 18 h. After completion, the reaction mixture was concentrated under vacuum to afford a yellow residue which was dissolved in water (30 mL)

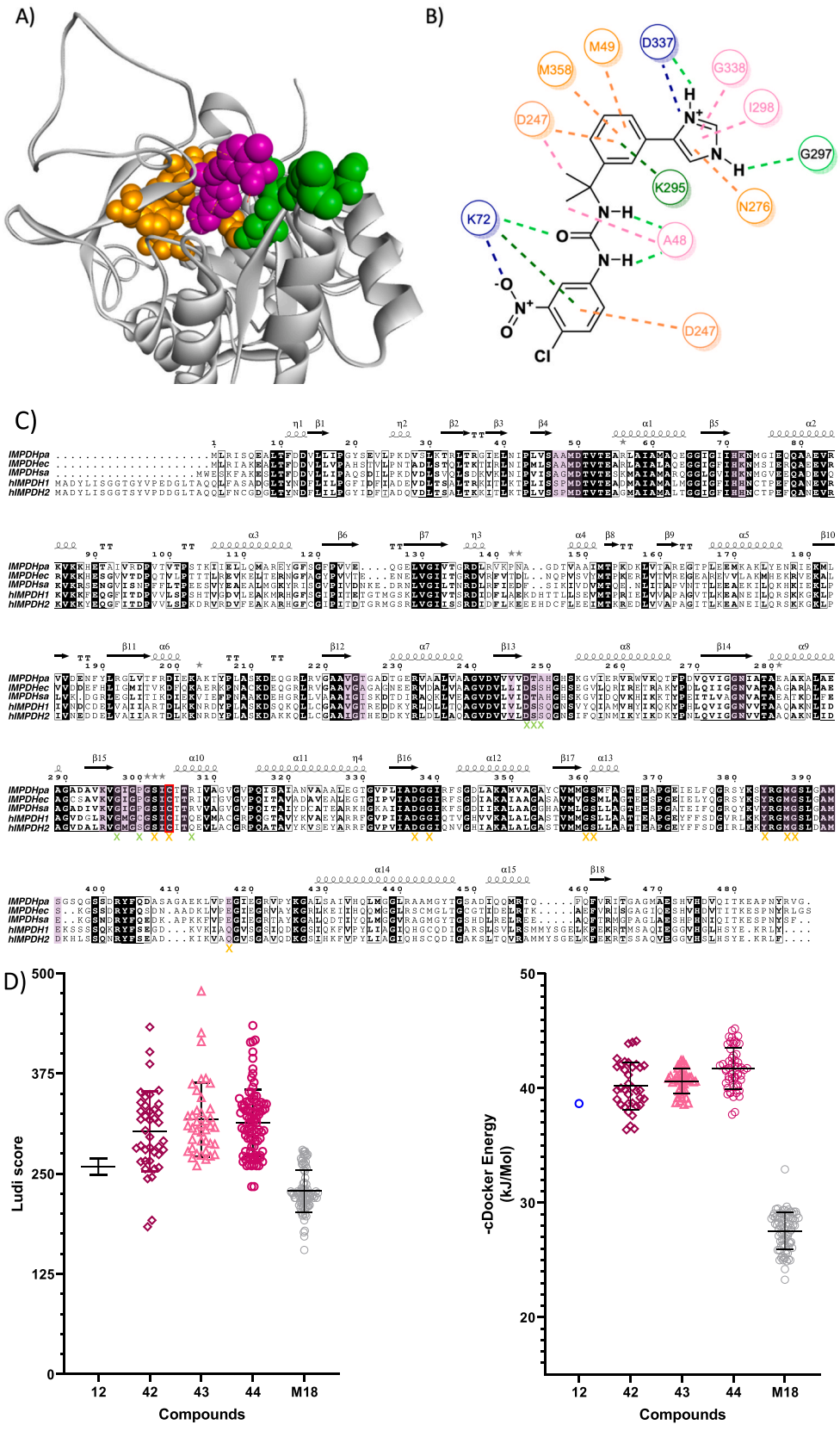

(caption on next page)

Fig. 7. Putative binding pocket of IMPDHpa ΔBD variant (pdb code 5AHL). A) The IMP binding site (orange), the NAD^+ binding site (green) and the putative inhibitor binding site (purple) highlighted within the catalytic domain of IMDPHpa. The ligand binding site partially overlaps with substrate binding sites without exhibiting full competitive binding. B) Binding pattern of **44**, the best scored ligand in docking experiments. Hydrogen bonds are shown in light green, cation-Pi interactions in dark green, salt bridge in blue, sigma-Pi interactions in orange and hydrophobic interactions in pink. C) Multiple sequence alignment of the three bacterial IMPDHs (IMPDHpa, IMPDHec and IMPDHsa), and the two human counterparts (hIMPDH1 and hIMPDH2). Residues interacting with IMP and NAD^+ are indicated by orange and green crosses, respectively. Potential binding sites of compounds **42**, **43** and **44** are highlighted in magenta. Conserved residues are shown in black blocks. Sequence alignment was performed using Clustal Omega [47] and ESPript 3.0 [48]. D) Clustering of ligands poses into the selected binding site. Full docked conformer poses showed better interaction scores for four urea derivatives (**12**, **42**, **43** and **44**) compared to **M18**. Filtering the poses for electrostatic interactions with Lys72 excluded **12** as an IMDPH ligand, as no complexes with electrostatic interactions were obtained between IMDPHpa and **12**.

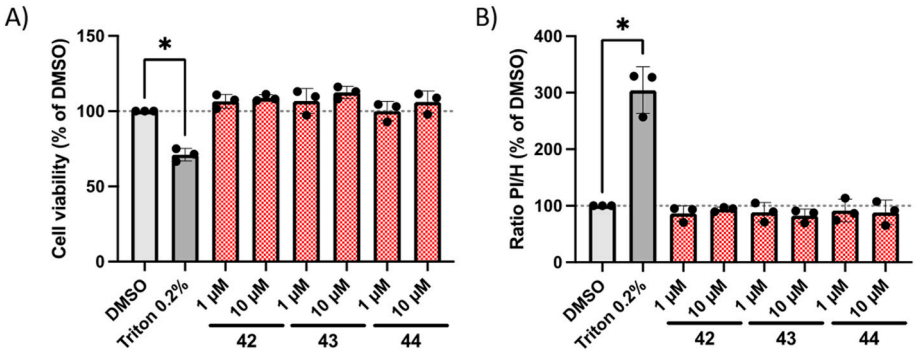

Fig. 8. After 72h of exposure to compounds **42**, **43** and **44** at 1 or 10 μM concentrations, cell viability and cell death were assessed by Alamar Blue assay (A) and measurement of PI/H staining ratio (B), respectively. DMSO at 0.1 % was used as vehicle and Triton X-100 0.2 % as positive control of cytotoxicity. Results are expressed as the mean ± SEM of three independent experiments; *p < 0.05 vs control (DMSO).

and extracted with ethyl acetate (2 X 25 mL). The combined organic layer was washed with a saturated solution of sodium bicarbonate (2 x 20 mL) and brine (1 x 20 mL). The organic layer was dried over magnesium sulfate and concentrated under vacuum to afford **6** as a colorless oil (5.50 g, 22.062 mmol, 97 %).

^{1}H NMR (400 MHz, $CDCl_3$): δ 1.24 (3H, t, J = 7.1 Hz, H10), 3.56 (2H, s, H7), 4.14 (2H, q, J = 7.0 Hz, H9), 7.14–7.21 (2H, m, H4, H3), 7.36 (1H, d, J = 7.3 Hz, H2), 7.43 (1H, s, H6).

^{13}C NMR (100 MHz, $CDCl_3$): δ 14.1 (C10), 40.9 (C7), 61.0 (C9) 122.4 (C1), 127.9 (C4), 130.0 (C3), 130.2 (C2), 132.3 (C6), 136.2 (C5), 170.8 (C8).

4.1.2. Synthesis of ethyl-2-(3-bromophenyl)-2-methylpropanoate (7) [25]

A solution of **6** (5.00 g, 20.568 mmol, 1.0 eq.) in tetrahydrofuran (50 mL) was cooled to 0 °C and sodium hydride (60 % in mineral oil, 2.05 g, 51.421 mmol, 2.5 eq.) was slowly added into the solution. The reaction mixture was stirred at the same temperature for 30 min and methyl iodide (3.2 mL, 51.421 mmol, 2.5 eq.) was added. The reaction mixture was then stirred at room temperature for 18 h. After completion, the reaction mixture was cooled to 0 °C and carefully quenched with ice. The reaction mixture was diluted with water (20 mL) and extracted with ethyl acetate (2 X 25 mL). The combined organic layer was washed with brine (20 mL) and dried over magnesium sulfate. The organic layer was concentrated under vacuum to afford **7** as a colorless oil (5.30 g, 19.546 mmol, 96 %).

^{1}H NMR (300 MHz, $CDCl_3$): δ 1.18 (3H, t, J = 7.1 Hz, H11), 1.55 (6H, s, H7), 4.12 (2H, q, J = 7.1 Hz, H10), 7.18 (1H, app. t, J = 7.9 Hz, H3), 7.26 (1H, d, J = 7.7 Hz, H4), 7.36 (1H, d, J = 7.5 Hz, H2), 7.48 (1H, br s, H6).

^{13}C NMR (75 MHz, $CDCl_3$): δ 14.0 (C11), 26.3 (C7), 46.4 (C8), 61.0 (C10) 122.5 (C1), 124.5 (C4), 128.9 (C3), 129.7 (C2), 129.8 (C6), 147.1 (C5), 176.0 (C9).

4.1.3. Synthesis of 2-(3-bromophenyl)-2-methylpropanoic acid (8) [25]

To a solution of **7** (5.30 g, 19.546 mmol, 1.0 eq.) in ethanol (50 mL) was added sodium hydroxide (3.90 g, 97.731 mmol, 5.0 eq.). The reaction mixture was heated to reflux at 80 °C for 18 h. After completion, the reaction mixture was concentrated under vacuum to produce a brown colored residue which was dissolved in water (20 mL) and extracted with diethyl ether (2 X 25 mL). The aqueous layer was acidified (pH = 1) using 1 N hydrochloric acid (30 mL) and extracted with ethyl acetate (3 X 25 mL). The combined organic layer was washed with brine (1 x 20 mL) and dried over magnesium sulfate. The organic layer was concentrated under vacuum to afford **8** as a brown solid (4.20 g, 17.277 mmol, 88 %).

^{1}H NMR (300 MHz, $CDCl_3$): δ 1.59 (6H, s, H7), 7.21 (1H, app. t, J = 7.8 Hz, H3), 7.32 (1H, ddd, J = 8.0 Hz, 1.9 Hz, 1.1 Hz, H4), 7.39 (1H, ddd, J = 7.8 Hz, 1.9 Hz, 1.0 Hz, H2), 7.53 (1H, app. t, J = 1.8 Hz, H6).

^{13}C NMR (100 MHz, $CDCl_3$): δ 25.1 (C7), 46.4 (C8), 121.6 (C1), 123.6 (C4), 128.1 (C3), 128.9 (C2), 129.1 (C6), 145.0 (C5), 181.3 (C9).

4.1.4. Synthesis of 1-benzyl-3-(2-(3-bromophenyl)propan-2-yl)urea (9)

To a solution of **8** (4.00 g, 16.454 mmol, 1.0 eq.) in dichloromethane (25 mL), cooled to 0 °C, was added triethylamine (2.9 mL, 21.391 mmol, 1.3 eq.). Ethylchloroformate (1.8 mL, 19.745 mmol, 1.2 eq.) was added dropwise and the reaction mixture was stirred at the same temperature for 1 h. Sodium azide (1.17 g, 18.100 mmol, 1.1 eq.) was added and the reaction mixture was stirred at room temperature for 18 h. After completion, the reaction mixture was filtered and the filtrate was concentrated under vacuum to afford 1-azido-2-(3-bromophenyl)-2-methylpropane-1-one as a brown colored oil. The azide intermediate which was then dissolved in toluene (20 mL) and heated to reflux for 2 h. The reaction mixture was concentrated under vacuum to afford 1-bromo-3-(2-isocyanatopropan-2-yl)benzene as a black colored oil (3.80 g, 15.827 mmol). A solution of 1-bromo-3-(2-isocyanatopropan-2-yl)benzene (3.80 g, 15.827 mmol, 1.0 eq.) in tetrahydrofuran (40 mL) was cooled to 0 °C and triethylamine (2.8 mL, 20.575 mmol, 1.3 eq.) was added. After stirring the reaction mixture for 10 min, benzylamine (2.0 mL, 18.992 mmol, 1.2 eq.) was added and the reaction mixture was stirred at room temperature for 18 h. After completion, the reaction mixture was diluted with water (20 mL) and extracted with ethyl acetate (2 X 30 mL). The combined organic layer was washed with brine (1 X 20 mL) and dried over magnesium sulfate. The organic layer was concentrated under vacuum to produce a residue which was purified by silica gel column chromatography using ethyl acetate-hexane (0 %–30 %) to afford urea intermediate **9** as a white solid (2.40 g, 6.891 mmol, 45 %).

^{1}H NMR (300 MHz, $CDCl_3$): δ 1.57 (6H, s, H7), 4.22 (2H, d, $J = 5.7$ Hz, H12), 4.60 (1H, t, $J = 5.4$ Hz, H11), 4.96 (1H, s, H9), 7.10–7.18 (3H, m, ArH), 7.24–7.35 (5H, m, ArH), 7.55 (1H, app. t, $J = 1.8$ Hz, H6).

^{13}C NMR (100 MHz, $CDCl_3$): δ 30.1 (C7), 44.0 (C12), 54.5 (C8), 122.7 (C1), 123.7 (ArC), 127.0 (ArC), 128.3 (ArC), 128.5 (ArC), 129.7 (ArC), 130.0 (ArC), 139.2 (C13), 149.9 (C5), 157.2 (C10). **IR (ATR, cm^{-1})**: 3330, 2924, 2865, 1634, 1557, 1453, 1382, 1262, 694.

HRMS (ESI$^+$): Exact mass calculated for $C_{17}H_{20}^{79}BrN_2O^+$ (M + H^+) 347.0754. Found: 347.0746.

4.1.5. General procedure for the synthesis of benzylurea derivatives (10–14)

A solution of **9** (1.0 eq.), the appropriate boronic acid/boronate ester (1.1 eq.), tripotassium phosphate (1.7 eq.) and triphenylphosphine (2 mol%) in dioxane (3.0 mL) and water (0.3 mL) was purged with nitrogen for 15 min. Tris(dibenzylideneacetone)dipalladium (1 mol%) was added and purging was continued for another 10 min. The resulting reaction mixture was heated via microwave irradiation to 100 °C for 1.5 h. The reaction mixture was diluted with water (10 mL) and extracted with ethyl acetate (2 X 20 mL). The combined organic layer was washed with brine (1 X 20 mL) and dried over magnesium sulfate. The organic layer was concentrated under vacuum to produce a residue which was purified by silica gel column chromatography using the stated eluent system.

4.1.6. Synthesis of 1-(2-(3-(1H-pyrazol-4-yl)phenyl)propan-2-yl)-3-benzylurea (10)

Prepared following the general procedure using **9** (100 mg, 0.288 mmol, 1.0 eq.), 4-(4,4,5,5-tetramethyl-1,3,2-dioxaborolan-2-yl)-1*H*-pyrazole (61 mg, 0.316 mmol, 1.1 eq.), tripotassium phosphate (104 mg, 0.489 mmol, 1.7 eq.), triphenylphosphine (2 mg, 0.006 mmol, 2 mol%) and tris(dibenzylideneacetone)dipalladium (2 mg, 0.002 mmol, 1 mol %). The residue was purified by silica gel column chromatography using methanol-dichloromethane (0 %–5 %) to afford **10** as a white solid (14 mg, 0.041 mmol, 15 %).

^{1}H NMR (400 MHz, DMSO-d_6): δ 1.57 (6H, s, H7), 4.14 (2H, d, $J =$ 5.2 Hz, H12), 6.30 (1H, br s, H11), 6.42 (1H, s, H9), 7.17–7.28 (8H, m, ArH), 7.38 (1H, d, $J = 7.4$ Hz, H2), 7.55 (1H, s, H6), 7.98 (2H, s, H20, H22).

^{13}C NMR (150 MHz, CD_3OD): δ 29.3 (C7), 42.9 (C12), 54.4 (C8), 121.8 (ArC), 122.6 (ArC), 122.8 (C19), 123.1 (ArC), 126.5 (ArC), 126.6 (ArC), 128.0 (C20, C22), 128.4 (ArC), 132.4 (C1), 140.1 (C13), 148.9 (C5), 158.4 (C10).

IR (ATR, cm^{-1}): 3321, 2925, 2854, 1644, 1609, 1555, 1380, 1263, 735.

HRMS (ESI$^+$): Exact mass calculated for $C_{20}H_{23}N_4O^+$ (M + H^+) 335.1866. Found: 335.1859.

Melting Point: 191–194 °C.

HPLC Purity: 98.0 %

4.1.7. Synthesis of 1-(2-(3-(1H-pyrazol-3-yl)phenyl)propan-2-yl)-3-benzylurea (11)

Prepared following the general procedure using **9** (100 mg, 0.288 mmol, 1.0 eq.), 3-(4,4,5,5-tetramethyl-1,3,2-dioxaborolan-2-yl)-1*H*-pyrazole (61 mg, 0.316 mmol, 1.1 eq.), tripotassium phosphate (104 mg, 0.489 mmol, 1.7 eq.), triphenylphosphine (2 mg, 0.006 mmol, 2 mol%) and tris(dibenzylideneacetone)dipalladium (2 mg, 0.002 mmol, 1 mol %). The residue was purified by silica gel column chromatography using methanol-dichloromethane (0 %–5 %) to afford **11** as a white solid (16 mg, 0.050 mmol, 17 %).

^{1}H NMR (400 MHz, DMSO-d_6): δ 1.59 (6H, s, H7), 4.16 (2H, s, H12), 6.29 (1H, br s, H11), 6.44 (1H, s, H9), 6.64 (1H, app. s, H20), 7.22–7.32 (7H, m, ArH), 7.58 (1H, d, $J = 6.3$ Hz, H21) 7.71 (1H, br s, H6), 7.83 (1H, s, H22).

^{13}C NMR (125 MHz, DMSO-d_6): δ 30.5 (C7), 42.9 (C12), 54.5 (C8), 122.2 (C20), 122.3 (ArC), 124.5 (ArC), 126.9 (ArC), 127.2 (ArC), 128.6 (ArC), 128.7 (C21), 141.4 (C1), 150.0 (C19), 157.5 (C10).

IR (ATR, cm^{-1}): 3316, 2923, 2852, 1641, 1609, 1559, 1381, 1261, 1086, 698.

HRMS (ESI$^+$): Exact mass calculated for $C_{20}H_{23}N_4O^+$ (M + H^+) 335.1866. Found: 335.1863.

Melting Point: 188–191 °C.

HPLC Purity: 98.1 %

4.1.8. Synthesis of 1-benzyl-3-(2-(3-(furan-2-yl)phenyl)propan-2-yl)urea (12)

Prepared following the general procedure using **9** (100 mg, 0.288 mmol, 1.0 eq.), furan-2-ylboronic acid (35 mg, 0.316 mmol, 1.1 eq.), tripotassium phosphate (104 mg, 0.489 mmol, 1.7 eq.), triphenylphosphine (2 mg, 0.006 mmol, 2 mol%) and tris(dibenzylideneacetone) dipalladium (2 mg, 0.002 mmol, 1 mol%). The residue was purified by silica gel column chromatography using ethyl acetate-hexane (0 %–25 %) to afford **12** as a white solid (10 mg, 0.029 mmol, 10 %).

^{1}H NMR (600 MHz, Acetone-d_6): δ 1.67 (6H, s, H7), 4.26 (2H, d, $J =$ 5.8 Hz, H12), 5.86 (1H,br s, H11), 6.03 (1H, s, H9), 6.54 (1H, dd, $J = 3.4$ Hz, 1.8 Hz, H21), 6.78 (1H, d, $J = 3.3$ Hz, H20), 7.17–7.27 (5H, m, ArH), 7.32 (1H, app. t, $J = 7.7$ Hz, H3), 7.37 (1H, d app. t, $J = 8.0$ Hz, 1.5 Hz, H4), 7.53 (1H, d app. t, $J = 7.7$ Hz, 1.6 Hz, H2), 7.61 (1H, d, $J = 1.6$ Hz, H22), 7.84 (1H, app. t, $J = 1.6$ Hz, H6).

^{13}C NMR (125 MHz, Acetone-d_6): δ 31.4 (C7), 44.8 (C12), 56.3 (C8), 106.7 (C20), 113.4 (C21), 122.2 (ArC), 123.1 (ArC), 126.0 (ArC), 128.2 (ArC), 128.8 (ArC), 129.9 (ArC), 130.1 (ArC), 132.3 (C1), 142.9 (C22), 143.9 (C13), 151.6 (C5), 156.0 (C19), 158.7 (C10).

IR (ATR, cm^{-1}): 3342, 2924, 1633, 1564, 1360, 1264, 1150, 1013, 697.

HRMS (ESI$^+$): Exact mass calculated for $C_{21}H_{23}N_2O_2^+$ (M + H^+) 335.1754. Found: 335.1753.

Melting Point: 150–152 °C.

HPLC Purity: 98.0 %

4.1.9. Synthesis of 1-benzyl-3-(2-(3-(thiophen-2-yl)phenyl)propan-2-yl) urea (13)

Prepared following the general procedure using **9** (50 mg, 0.144 mmol, 1.0 eq.), thiophen-2-ylboronic acid (20 mg, 0.158 mmol, 1.1 eq.), tripotassium phosphate (52 mg, 0.244 mmol, 1.7 eq), triphenylphosphine (1 mg, 0.003 mmol, 2 mol%) and tris(dibenzylideneacetone) dipalladium (1 mg, 0.001 mmol, 1 mol%). The residue was purified by silica gel column chromatography using ethyl acetate-hexane (0 %–25 %) to afford **13** as a white solid (25 mg, 0.071 mmol, 50 %).

^{1}H NMR (600 MHz, Acetone-d_6): δ 1.67 (6H, s, H7), 4.26 (2H, d, $J =$ 5.7 Hz, H12), 5.89 (1H, br s, H11), 6.06 (1H, s, H9), 7.11 (1H, dd, $J =$ 5.0 Hz, 3.5 Hz, H21), 7.18 (1H, m, ArH), 7.22–7.23 (4H, m, ArH), 7.31 (1H, app. t, $J = 7.6$ Hz, H3), 7.38–7.39 (2H, m, ArH), 7.43 (1H, dd, $J =$ 4.9 Hz, 1.2 Hz, H22), 7.46 (1H, d app. t, $J = 7.6$ Hz, 1.5 Hz, H2), 7.77 (1H, app. t, $J = 1.7$ Hz, H6).

^{13}C NMR (100 MHz, Acetone-d_6): δ 31.4 (C7), 44.8 (C12), 56.2 (C8), 124.3 (ArC), 124.9 (ArC), 125.0 (ArC), 126.2 (ArC), 126.5 (ArC), 128.2 (C20), 128.8 (ArC), 129.8 (C21), 129.9 (ArC), 130.3 (C22), 135.7 (C1), 142.9 (C13), 146.4 (C5), 151.9 (C19), 158.7 (C10).

R (ATR, cm^{-1}): 3337, 2972, 2824, 1635, 1553, 1453, 1361, 1273, 697.

HRMS (ESI$^+$): Exact mass calculated for $C_{21}H_{23}N_2OS^+$ (M + H^+) 351.1526. Found: 351.1523.

Melting Point: 158–160 °C.

HPLC Purity: 98.8 %

4.1.10. Synthesis of 1-(2-([1,1′-biphenyl]-3-yl)propan-2-yl)-3-benzylurea (14)

Prepared following the general procedure using **9** (50 mg, 0.144 mmol, 1.0 eq.), phenylboronic acid (19 mg, 0.158 mmol, 1.1 eq.), tripotassium phosphate (52 mg, 0.244 mmol, 1.7 eq.), triphenylphosphine (1 mg, 0.003 mmol, 2 mol%) and tris(dibenzylideneacetone)dipalladium (1 mg, 0.001 mmol, 1 mol%). The residue was purified by silica gel

column chromatography using ethyl acetate-hexane (0 %–30 %) to afford **14** as a white solid (10 mg, 0.026 mmol, 20 %).

^{1}H NMR (600 MHz, $CDCl_3$): δ 1.68 (6H, s, H7), 4.25 (2H, d, $J = 5.3$ Hz, H12), 4.53 (1H, br s, H11), 5.01 (1H, s, H9), 7.03–7.04 (2H, m, ArH), 7.17–7.18 (3H, m, ArH), 7.37–7.49 (6H, m, ArH), 7.53 (2H, d, $J = 7.3$ Hz, ArH), 7.68 (1H, s, H6).

^{13}C NMR (150 MHz, $CDCl_3$): δ 30.4 (C7), 44.1 (C12), 54.9 (C8), 124.2 (ArC), 124.3 (ArC), 126.0 (ArC), 127.0 (ArC), 127.29 (ArC), 127.4 (ArC), 128.4 (ArC), 128.7 (ArC), 129.2 (ArC), 139.0 (C13), 141.1 (ArC), 141.7 (ArC), 147.0 (C5), 157.3 (C10).

IR (ATR, cm^{-1}): 3339, 2972, 2865, 1636, 1552, 1452, 1381.

HRMS (ESI$^+$): Exact mass calculated for $C_{23}H_{25}N_2O^+$ (M + H$^+$) 345.1961. Found: 345.1959.

Melting Point: 152–155 °C.

HPLC Purity: 97.1 %

4.1.11. Synthesis of ethyl 2-methyl-2-(3-(4,4,5,5-tetramethyl-1,3,2-dioxaborolan-2-yl)phenyl)propanoate (15)

A solution of **7** (200 mg, 0.738 mmol, 1.0 eq.), bis(pinacolato) diboron (225 mg, 0.885 mmol, 1.2 eq.) and potassium acetate (217 mg, 2.214 mmol, 3.0 eq) in dimethoxyethane (5.0 mL) was purged with nitrogen for 15 min. Palladium chloride (13 mg, 0.073 mmol, 0.1 eq.) and 1,1′-bis(diphenylphosphino)ferrocene (41 mg, 0.073 mmol, 0.1 eq.) was added and purging was continued for another 10 min. The reaction mixture was stirred at 90 °C for 18 h. After completion, the reaction mixture was concentrated under vacuum and the resulting residue was purified by silica gel column chromatography using ethyl acetate-hexane (0 %–15 %) to afford **15** as a white solid (165 mg, 0.518 mmol, 70 %).

^{1}H NMR (400 MHz, $CDCl_3$): δ 1.18 (3H, t, $J = 7.1$ Hz, H11), 1.34 (12H, s, H12, H13), 1.59 (6H, s, H7), 4.12 (2H, q, $J = 6.9$ Hz, H10), 7.32 (1H, app. t, $J = 7.6$ Hz, H3), 7.41 (1H, d, $J = 7.8$ Hz, H4), 7.68 (1H, d, $J = 7.1$ Hz, H2), 7.78 (1H, s, H6).

^{13}C NMR (100 MHz, $CDCl_3$): δ 14.0 (C11), 24.8 (C12, C13), 26.6 (C7), 46.5 (C8), 60.7 (C10), 83.7 (C14), 127.7 (ArC), 128.8 (ArC), 131.5 (C1), 133.1 (ArC), 144.0 (ArC), 176.8 (C9).

HRMS (ESI$^+$): Exact mass calculated for $C_{18}H_{28}BO_4^+$ (M + H$^+$) 319.2075. Found: 319.2076.

4.1.12. General procedure for the synthesis of substituted dimethyl ester derivatives (16–23)

A solution of **7** or **15** (1.0 eq.), the appropriate boronic acid/boronate ester or bromide (1.2 eq.) and sodium carbonate (3.0 eq.) in acetonitrile (5.0 mL) and water (0.5 mL) was purged with nitrogen for 15 min. Tetrakis(triphenylphosphine)palladium (6 mol%) was added and purging was continued for another 10 min. The resulting reaction mixture was heated via microwave irradiation to 100 °C for 1.5 h. After completion, the reaction mixture was concentrated under vacuum and the resulting residue was purified by silica gel column chromatography using the stated eluent system.

4.1.13. Synthesis of ethyl 2-(3-(1H-pyrazol-4-yl)phenyl)-2-methylpropanoate (16)

Prepared following the general procedure using **7** (200 mg, 0.738 mmol, 1.0 eq.), 4-(4,4,5,5-tetramethyl-1,3,2-dioxaborolan-2-yl)-1*H*-pyrazole (171 mg, 0.885 mmol, 1.2 eq.), sodium carbonate (234 mg, 2.214 mmol, 3.0 eq.) and tetrakis(triphenylphosphine)palladium (51 mg, 0.738 mmol, 6 mol%). The residue was purified by silica gel column chromatography using ethyl acetate-hexane (0 %–40 %) to afford **16** as a colorless oil (114 mg, 0.541 mmol, 60 %).

^{1}H NMR (400 MHz, $CDCl_3$): δ 1.10 (3H, t, $J = 7.1$ Hz, H11), 1.52 (6H, s, H7), 4.05 (2H, q, $J = 6.8$ Hz, H10), 7.13 (1H, d, $J = 7.6$ Hz, H4), 7.22 (1H, app. t, $J = 7.6$ Hz, H3), 7.29 (1H, d, $J = 7.4$ Hz, H2), 7.39 (1H, s, H6), 7.79 (2H, s, H12, H14), 9.03 (1H, br s, H13).

^{13}C NMR (100 MHz, $CDCl_3$): δ 14.0 (C11), 26.5 (C7), 46.5 (C8), 60.9 (C10), 123.1 (ArC), 123.9 (ArC), 124.2 (ArC), 128.9 (C15), 131.1 (C12, C14), 132.6 (C5), 145.4 (C1), 176.8 (C9).

IR (ATR, cm^{-1}): 3180, 2930, 1723, 1366, 1254, 1146, 701.

HRMS (ESI$^+$): Exact mass calculated for $C_{15}H_{19}N_2O_2^+$ (M + H$^+$) 259.1441. Found: 259.1440.

4.1.14. Synthesis of ethyl 2-(3-(1H-pyrazol-3-yl)phenyl)-2-methylpropanoate (17)

Prepared following the general procedure using **7** (200 mg, 0.738 mmol, 1.0 eq.), 3-(4,4,5,5-tetramethyl-1,3,2-dioxaborolan-2-yl)-1*H*-pyrazole (171 mg, 0.885 mmol, 1.2 eq.), sodium carbonate (234 mg, 2.214 mmol, 3.0 eq.) and tetrakis(triphenylphosphine)palladium (51 mg, 0.738 mmol, 6 mol%). The residue was purified by silica gel column chromatography using ethyl acetate-hexane (0 %–40 %) to afford **17** as a colorless oil (180 mg, 0.696 mmol, 95 %).

^{1}H NMR (600 MHz, $CDCl_3$): δ 1.18 (3H, t, $J = 7.2$ Hz, H11), 1.25 (6H, s, H7), 4.12 (2H, q, $J = 7.0$ Hz, H10), 6.06 (1H, br s, H14), 7.30 (1H, d, $J = 7.9$ Hz, H4), 7.37 (1H, app. t, $J = 7.5$ Hz, H3), 7.61–7.63 (2H, m, ArH), 7.76 (1H, s, H6).

^{13}C NMR (100 MHz, $CDCl_3$): δ 14.0 (C11), 26.5 (C7), 46.5 (C8), 61.9 (C10), 102.9 (C14), 123.1 (ArC), 124.2 (ArC), 125.7 (ArC), 128.8 (C13), 131.8 (C5), 145.4 (C15), 176.6 (C9).

IR (ATR, cm^{-1}): 3204, 2976, 1725, 1609, 1385, 1256, 1147, 767.

HRMS (ESI$^+$): Exact mass calculated for $C_{15}H_{19}N_2O_2^+$ (M + H$^+$) 259.1441. Found: 259.1441.

4.1.15. Synthesis of ethyl 2-methyl-2-(3-(thiophen-2-yl)phenyl)propanoate (18)

Prepared following the general procedure using **7** (200 mg, 0.738 mmol, 1.0 eq.), thiophen-2-ylboronic acid (112 mg, 0.885 mmol, 1.2 eq.), sodium carbonate (234 mg, 2.214 mmol, 3.0 eq.), and tetrakis (triphenylphosphine)palladium (51 mg, 0.738 mmol, 6 mol%). The residue was purified by silica gel column chromatography using ethyl acetate-hexane (0 %–15 %) to afford **18** as a colorless oil (170 mg, 0.619 mmol, 84 %).

^{1}H NMR (400 MHz, $CDCl_3$): δ 1.11 (3H, t, $J = 7.2$ Hz, H11), 1.52 (6H, s, H7), 4.05 (2H, q, $J = 7.2$ Hz, H10), 6.98 (1H, dd, $J = 5.0$ Hz, 3.6 Hz, H13), 7.17–7.24 (4H, m, ArH), 7.39 (1H, d, $J = 7.7$ Hz, H2), 7.49 (1H, br s, H6).

^{13}C NMR (100 MHz, $CDCl_3$): δ 14.1 (C11), 26.5 (C7), 46.5 (C8), 60.9 (C10), 123.2 (ArC), 123.4 (ArC), 124.4 (ArC), 124.8 (C12), 128.0 (C13), 128.9 (C14), 134.4 (ArC), 144.5 (C15), 145.5 (ArC), 176.5 (C9).

IR (ATR, cm^{-1}): 3442, 2977, 1724, 1385, 1252, 1144, 852, 699.

HRMS (ESI$^+$): Exact mass calculated for $C_{16}H_{19}O_2SNa^+$ (M + Na$^+$) 297.0920. Found: 297.0906.

4.1.16. Synthesis of ethyl 2-(3-(furan-2-yl)phenyl)-2-methylpropanoate (19)

Prepared following the general procedure using **7** (200 mg, 0.738 mmol, 1.0 eq.), furan-2-ylboronic acid (99 mg, 0.885 mmol, 1.2 eq.), sodium carbonate (234 mg, 2.214 mmol, 3.0 eq.) and tetrakis(triphenylphosphine)palladium (51 mg, 0.738 mmol, 6 mol%). The residue was purified by silica gel column chromatography using ethyl acetate-hexane (0 %–15 %) to afford **19** as a colorless oil (150 mg, 0.580 mmol, 79 %).

^{1}H NMR (400 MHz, $CDCl_3$): δ 1.10 (3H, t, $J = 7.1$ Hz, H11), 1.52 (6H, s, H7), 4.04 (2H, q, $J = 6.9$ Hz, H10), 6.37 (1H, dd, $J = 3.3$ Hz, 1.7 Hz, H13), 6.55 (1H, d, $J = 3.2$ Hz, H12), 7.14 (1H, d, $J = 7.5$ Hz, H4), 7.24 (1H, app. t, $J = 7.7$ Hz, H3), 7.36 (1H, d, $J = 1.5$ Hz, H14), 7.45 (1H, d, $J = 7.6$ Hz, H2), 7.58 (1H, s, H6).

^{13}C NMR (100 MHz, $CDCl_3$): δ 14.0 (C11), 26.5 (C7), 46.5 (C8), 60.8 (C10), 105.0 (C12), 111.6 (C13), 121.1 (C4), 122.2 (C3), 124.7 (C2), 128.7 (C1), 130.9 (C6), 142.0 (C5), 145.3 (C14), 154.0 (C15), 176.5 (C9).

IR (ATR, cm^{-1}): 2978, 1726, 1366, 1257, 1147, 697.

HRMS (ESI$^+$): Exact mass calculated for $C_{16}H_{19}O_3^+$ (M + H$^+$) 259.1329. Found: 259.1322.

4.1.17. Synthesis of ethyl 2-(3-(2-fluoropyridin-3-yl)phenyl)-2-methylpropanoate (20)

Prepared following the general procedure using **7** (200 mg, 0.738 mmol, 1.0 eq.), (2-fluoropyridin-3-yl)boronic acid (125 mg, 0.885 mmol, 1.2 eq.), sodium carbonate (234 mg, 2.214 mmol, 3.0 eq.), and tetrakis(triphenylphosphine)palladium (51 mg, 0.738 mmol, 6 mol%). The residue was purified by silica gel column chromatography using ethyl acetate-hexane (0 %–15 %) to afford **20** as a colorless oil (200 mg, 0.696 mmol, 94 %).

^{1}H NMR (400 MHz, $CDCl_3$): δ 1.12 (3H, t, $J = 7.1$ Hz, H11), 1.54 (6H, s, H7), 4.06 (2H, q, $J = 7.2$ Hz, H10), 7.19–7.21 (1H, m, H3), 7.33–7.36 (3H, m, ArH), 7.45 (1H, br s, H6), 7.78 (1H, dd, $J = 7.6$ Hz, 3.2 Hz, H14), 8.11 (1H, d, $J = 3.5$ Hz, H13).

^{13}C NMR (100 MHz, $CDCl_3$): δ 14.0 (C11), 26.5 (C7), 46.5 (C8), 60.9 (C10), 121.7 (d, $^4J_{C\text{-}F} = 4.5$ Hz, C14), 123.9 (d, $^2J_{C\text{-}F} = 28.3$ Hz, C16), 125.8 (C3), 126.3 (d, $^4J_{C\text{-}F} = 3.0$ Hz, C6), 127.1 (d, $^4J_{C\text{-}F} = 2.9$ Hz, C2), 128.7 (C4), 133.9 (d, $^3J_{C\text{-}F} = 4.9$ Hz, C1), 140.7 (d, $^3J_{C\text{-}F} = 4.3$ Hz, C15), 145.4 (C5), 146.3 (d, $^3J_{C\text{-}F} = 14.5$ Hz, C13), 160.5 (d, $^1J_{C\text{-}F} = 242.4$ Hz, C12), 176.4 (C9).

^{19}F NMR (376 MHz, $CDCl_3$): δ −71.04 (s, C–F).

IR (ATR, cm^{-1}): 2929, 2850, 1726, 1584, 1433, 1399, 1249, 1146, 794.

HRMS (ESI$^+$): Exact mass calculated for $C_{17}H_{19}FNO_2^+$ (M + H$^+$) 288.1394. Found: 288.1389.

4.1.18. Synthesis of ethyl 2-methyl-2-(3-(thiazol-2-yl)phenyl)propanoate (21)

Prepared following the general procedure using **15** (200 mg, 0.628 mmol, 1.0 eq.), 2-bromothiazole (0.067 mL, 0.754 mmol, 1.2 eq.), sodium carbonate (196 mg, 1.885 mmol, 3.0 eq.), and tetrakis(triphenylphosphine)palladium (43 mg, 0.037 mmol, 6 mol%). The residue was purified by silica gel column chromatography using ethyl acetate-hexane (0 %–15 %) to afford **21** as a colorless oil (158 mg, 0.573 mmol, 92 %).

^{1}H NMR (400 MHz, $CDCl_3$): δ 1.09 (3H, t, $J = 6.9$ Hz, H11), 1.54 (6H, s, H7), 4.05 (2H, q, $J = 7.3$ Hz, H10), 7.22 (1H, d, $J = 3.3$ Hz, H13), 7.30–7.31 (2H, m, ArH), 7.70–7.73 (1H, m, H3), 7.76 (1H, d, $J = 3.3$ Hz, H12), 7.90 (1H, s, H6).

^{13}C NMR (100 MHz, $CDCl_3$): δ 13.0 (C11), 25.4 (C7), 45.4 (C8), 59.8 (C10), 117.8 (C13), 122.7 (ArC), 124.0 (ArC), 126.6 (ArC), 127.9 (ArC), 132.5 (C1), 142.5 (ArC), 142.8 (ArC), 144.7 (C12), 167.3 (C14), 175.3 (C9).

IR (ATR, cm^{-1}): 3443, 2977, 1725, 1385, 1252, 1143, 858, 697.

HRMS (ESI$^+$): Exact mass calculated for $C_{15}H_{18}NO_2S^+$ (M + H$^+$) 276.1053. Found: 276.1050.

4.1.19. Synthesis of ethyl 2-methyl-2-(3-(1-trityl-1H-imidazole-4-yl) phenyl)propanoate (22)

Prepared following the general procedure using **15** (300 mg, 0.943 mmol, 1.0 eq.), 4-bromo-1-trityl-1*H*-imidazole (440 mg, 1.132 mmol, 1.2 eq.), sodium carbonate (299 mg, 2.830 mmol, 3.0 eq.), and tetrakis (triphenylphosphine)palladium (65 mg, 0.056 mmol, 6 mol%). The residue was purified by silica gel column chromatography using ethyl acetate-hexane (0 %–15 %) to afford **22** as a colorless oil (215 mg, 0.423 mmol, 45 %).

^{1}H NMR (300 MHz, $CDCl_3$): δ 1.15 (3H, t, $J = 7.0$ Hz, H11), 1.59 (6H, s, H7), 4.10 (2H, q, $J = 7.1$ Hz, H10), 7.11 (1H, d, $J = 1.4$ Hz, H13), 7.17–7.22 (7H, m, ArH), 7.25 (1H, d, $J = 1.6$ Hz, H14), 7.32–7.36 (9H, m, ArH), 7.52–7.56 (2H, m, ArH), 7.77 (1H, app. t, $J = 1.5$ Hz, H6).

^{13}C NMR (75 MHz, $CDCl_3$): δ 14.0 (C11), 26.5 (C7), 46.6 (C8), 60.7 (C10), 75.6 (C15), 117.4 (C13), 121.9 (ArC), 123.2 (ArC), 124.5 (ArC), 128.1 (ArC), 128.2 (ArC), 128.5 (ArC), 129.8 (C14), 133.9 (ArC), 139.1 (C1), 140.7 (C12), 142.2 (ArC), 145.2 (C5), 176.8 (C9).

IR (ATR, cm^{-1}): 3360, 2973, 1726, 1491, 1384, 1256, 701.

HRMS (ESI$^+$): Exact mass calculated for $C_{34}H_{33}N_2O_2^+$ (M + H$^+$) 501.2537. Found: 501.2533.

4.1.20. Synthesis of ethyl 2-(3-(1-benzyl-1H-imidazole-2-yl)phenyl)-2-methylpropanoate (23)

Prepared following the general procedure using **15** (200 mg, 0.628 mmol, 1.0 eq.), 1-benzyl-2-bromo-1*H*-imidazole (178 mg, 0.754 mmol, 1.2 eq.), sodium carbonate (199 mg, 1.886 mmol, 3.0 eq.), and tetrakis (triphenylphosphine)palladium (43 mg, 0.037 mmol, 6 mol%). The residue was purified by silica gel column chromatography using methanol-dichloromethane (0 %–1 %) to afford **23** as a colorless oil (96 mg, 0.275 mmol, 44 %).

^{1}H NMR (300 MHz, $CDCl_3$): δ 1.14 (3H, t, $J = 7.1$ Hz, H11), 1.49 (6H, s, H7), 4.06 (2H, q, $J = 7.2$ Hz, H10), 5.21 (2H, s, H14), 6.99 (1H, d, $J = 1.2$ Hz, H12), 7.07–7.09 (2H, m, ArH), 7.21 (1H, d, $J = 1.3$ Hz, H13), 7.30–7.45 (6H, m, ArH), 7.52 (1H, br s, H6).

^{13}C NMR (100 MHz, $CDCl_3$): δ 14.0 (C11), 26.3 (C7), 46.4 (C8), 50.4 (C14), 60.8 (C10), 121.3 (C13), 126.2 (ArC), 126.4 (ArC), 126.7 (ArC), 127.1 (ArC), 128.0 (ArC), 128.4 (C12), 128.6 (ArC), 129.0 (ArC), 129.9 (ArC), 136.7 (C1), 145.3 (ArC), 148.2 (C15), 176.3 (C9).

IR (ATR, cm^{-1}): 2976, 1732, 1453, 1385, 1253, 1144, 703.

HRMS (ESI$^+$): Exact mass calculated for $C_{22}H_{25}N_2O_2^+$ (M + H$^+$) 349.1911. Found: 349.1911.

4.1.21. General procedure for the synthesis of α,α-dimethylcarboxylic acids (24–31)

A solution of ester (1.0 eq.) and sodium hydroxide (5.0 eq.) in ethanol (5.0 mL) was heated to reflux at 80 °C for 18 h. After completion, the reaction mixture was concentrated under vacuum. The residue was dissolved in water (15 mL) and extracted with diethyl ether (2 X 20 mL). The aqueous layer was acidified (pH 1) with 2 N hydrochloric acid and extracted with ethyl acetate (2 X 20 mL). The combined organic layer was washed with brine (20 mL) and dried over magnesium sulfate. The organic layer was concentrated under vacuum to afford the target dimethyl carboxylic acid.

4.1.22. Synthesis of 2-(3-(1H-pyrazol-4-yl)phenyl)-2-methylpropanoic acid (24)

Prepared following the general procedure using **16** (114 mg, 0.441 mmol, 1.0 eq.) and sodium hydroxide (88 mg, 2.206 mmol, 5.0 eq.). Following work-up, **24** was recovered as a colorless oil (100 mg, 0.434 mmol, 98 %).

^{1}H NMR (400 MHz, CD_3OD): δ 1.60 (6H, s, H7), 7.26 (1H, d, $J = 7.4$ Hz, H4), 7.32 (1H, app. t, $J = 7.4$ Hz, H3), 7.44 (1H, d, $J = 7.1$ Hz, H2), 7.58 (1H, br s, H6), 8.01 (2H, s, H10, H12).

^{13}C NMR (100 MHz, CD_3OD): δ 27.1 (C7), 47.5 (C8), 124.1 (C13), 125.0 (ArC), 125.1 (ArC), 129.9 (C10, C12), 132.3 (ArC), 133.8 (ArC), 147.0 (C13), 180.6 (C9).

IR (ATR, cm^{-1}): 3295, 2923, 2856, 1698, 1602, 1369, 1263, 698.

HRMS (ESI$^+$): Exact mass calculated for $C_{13}H_{15}N_2O_2^+$ (M + H$^+$) 231.1128. Found: 231.1126.

4.1.23. Synthesis of 2-(3-(1H-pyrazol-3-yl)phenyl)-2-methylpropanoic acid (25)

Prepared following the general procedure using **17** (180 mg, 0.696 mmol, 1.0 eq.) and sodium hydroxide (278 mg, 3.484 mmol, 5.0 eq.). Following work-up, **25** was recovered as a brown solid (112 mg, 0.486 mmol, 70 %).

^{1}H NMR (400 MHz, DMSO-d_6): δ 1.52 (6H, s, H7), 6.69 (1H, d, $J = 1.9$ Hz, H13), 7.27 (1H, d, $J = 7.7$ Hz, H4), 7.37 (1H, app. t, $J = 7.7$ Hz, H3), 7.64 (1H, d, $J = 7.8$ Hz,H2), 7.72 (1H, d, $J = 2.1$ Hz, H12), 7.79 (1H, br s, H6).

^{13}C NMR (125 MHz, DMSO-d_6): δ 26.8 (C7), 46.2 (C8), 102.4 (C13), 122.8 (ArC), 122.9 (ArC), 123.9 (ArC), 125.2 (ArC), 129.0 (C12), 145.9 (C14), 177.9 (C9).

IR (ATR, cm^{-1}): 3139, 2923, 2853, 1701, 1466, 1365, 697.

HRMS (ESI$^+$): Exact mass calculated for $C_{20}H_{22}N_4O$ (M + H$^+$) 231.1129. Found: 231.1134.

4.1.24. Synthesis of 2-methyl-2-(3-(thiophen-2-yl)phenyl)propanoic acid (26)

Prepared following the general procedure using **18** (170 mg, 0.619 mmol, 1.0 eq.) and sodium hydroxide (124 mg, 3.098 mmol, 5.0 eq.). Following work-up, **26** was recovered as an off-white solid (143 mg, 0.580 mmol, 94 %).

^{1}H NMR (400 MHz, $CDCl_3$): δ 1.54 (6H, s, H7), 6.95 (1H, dd, $J = 5.0$ Hz, 3.6 Hz, H11), 7.15 (1H, d, $J = 5.1$ Hz, H10), 7.15–7.23 (3H, m, ArH), 7.38–7.40 (1H, m, H3), 7.54 (1H, br s, H6), 11.33 (1H, br s, H14).

^{13}C NMR (100 MHz, $CDCl_3$): δ 26.2 (C7), 46.3 (C8), 123.4 (ArC), 123.6 (C12), 124.8 (ArC), 125.0 (ArC), 125.2 (C10), 128.0 (C11), 129.1 (C12), 134.6 (ArC), 144.3 (ArC), 144.5 (C13), 183.9 (C9).

IR (ATR, cm^{-1}): 3071, 2976, 1697, 1366, 1289, 854, 697.

HRMS (ESI$^+$): Exact mass calculated for $C_{14}H_{15}O_2S^+$ (M + H^+) 247.0787. Found: 247.0787.

4.1.25. Synthesis of 2-(3-(furan-2-yl)phenyl)-2-methylpropanoic acid (27)

Prepared following the general procedure using **19** (150 mg, 0.581 mmol, 1.0 eq.) and sodium hydroxide (116 mg, 2.905 mmol, 5.0 eq.). Following work-up, **27** was recovered as an off-white solid (110 mg, 0.477 mmol, 83 %).

^{1}H NMR (400 MHz, $CDCl_3$): δ 1.54 (6H, s, H7), 6.35 (1H, dd, $J = 3.0$ Hz, 1.7 Hz, H11), 6.55 (1H, d, $J = 3.1$ Hz, H10), 7.19–7.27 (2H, m, H3, H4), 7.35 (1H, d, $J = 1.5$ Hz, H12), 7.46 (1H, d, $J = 7.4$ Hz, H2), 7.63 (1H, s, H6), 9.94 (1H, br s, H14).

^{13}C NMR (100 MHz, $CDCl_3$): δ 26.2 (C7), 46.3 (C8), 105.3 (C10), 111.7 (C11), 121.3 (ArC), 122.6 (ArC), 125.0 (ArC), 128.8 (ArC), 131.0 (ArC), 142.1 (ArC), 144.3 (C12), 153.8 (C13), 183.3 (C9).

IR (ATR, cm^{-1}): 3268, 2976, 2847, 1697, 1367, 1158, 797.

HRMS (ESI$^+$): Exact mass calculated for $C_{14}H_{15}O_3^+$ (M + H^+) 231.1016. Found: 231.1014.

4.1.26. Synthesis of 2-methyl-2-(3-(thiazol-2-yl)phenyl)propanoic acid (28)

Prepared following the general procedure using **21** (158 mg, 0.573 mmol, 1.0 eq.) and sodium hydroxide (114 mg, 2.868 mmol, 5.0 eq.). After work-up, **28** was recovered as an off-white solid (110 mg, 0.444 mmol, 78 %).

^{1}H NMR (400 MHz, $CDCl_3$): δ 1.57 (6H, s, H7), 7.20 (1H, br s, H12), 7.28 (1H, app. t, $J = 6.6$ Hz, H3), 7.39 (1H, d, $J = 6.6$ Hz, H4), 7.64 (1H, d, $J = 6.8$ Hz, H2), 7.85 (1H, s, H6), 8.0 (1H, br s, H11), 11.4 (1H, br s, H10).

^{13}C NMR (100 MHz, $CDCl_3$): δ 25.2 (C7), 45.3 (C8), 117.9 (C12), 123.1 (ArC), 124.4 (C3), 127.0 (C4), 128.0 (C2), 131.9 (C1), 142.3 (ArC), 144.3 (C11), 167.8 (C13), 180.1 (C9).

IR (ATR, cm^{-1}): 3253, 2924, 2850, 1700, 1145, 797, 695.

HRMS (ESI$^+$): Exact mass calculated for $C_{13}H_{14}NO_2S^+$ (M + H^+) 248.0740. Found: 248.0732.

4.1.27. Synthesis of 2-methyl-2-(3-(1-trityl-1H-imidazole-4-yl)phenyl) propanoic acid (29)

Prepared following the general procedure using **22** (215 mg, 0.429 mmol, 1.0 eq.) and sodium hydroxide (86 mg, 2.147 mmol, 5.0 eq.). Following work-up, **29** was recovered as an off-white solid (200 mg, 0.423 mmol, 98 %).

^{1}H NMR (300 MHz, $CDCl_3$): δ 1.56 (6H, s, H7), 7.00–7.08 (7H, m, ArH), 7.18–7.37 (13H, m, ArH), 7.80 (1H, s, H6), 8.10 (1H, s, H14), 8.85 (1H, br s, H10).

^{13}C NMR (100 MHz, $CDCl_3$): δ 26.4 (C7), 46.4 (C8), 77.2 (C15), 117.7 (C13), 123.7 (ArC), 125.7 (ArC), 127.9 (ArC), 128.5 (ArC), 128.6 (ArC), 129.7 (C14), 138.0 (C1), 141.0 (C12), 145.9 (C5), 180.0 (C9).

IR (ATR, cm^{-1}): 3708, 2967, 2844, 1327, 1259, 1032, 698.

HRMS (ESI$^+$): Exact mass calculated for $C_{32}H_{29}N_2O_2^+$ (M + H^+) 473.2224. Found: 473.2211.

4.1.28. Synthesis of 2-(3-(1-benzyl-1H-imidazole-2-yl)phenyl)-2-methylpropanoic acid (30)

Prepared following the general procedure using **23** (138 mg, 0.396 mmol, 1.0 eq.) and sodium hydroxide (79 mg, 1.981 mmol, 5.0 eq.). Following work-up, **30** was recovered as a colorless oil (50 mg, 0.156 mmol, 40 %).

^{1}H NMR (300 MHz, $CDCl_3$): δ 1.63 (6H, s, H7), 5.26 (2H, s, H13), 7.01 (1H, d, $J = 1.1$ Hz, H11), 7.14–7.17 (2H, m, ArH), 7.35–7.44 (6H, m, ArH), 7.57 (1H, d, $J = 6.8$ Hz, H2), 7.76 (1H, s, H6), 10.47 (1H, br s, H10).

^{13}C NMR (75 MHz, $CDCl_3$): δ 26.4 (C7), 46.5 (C8), 50.5 (C13), 60.8 (C10), 113.7 (ArC), 113.9 (ArC), 116.7 (ArC), 121.1 (C12), 126.6 (ArC), 127.3 (ArC), 127.5 (ArC), 127.9 (ArC), 128.13 (C11), 128.4 (ArC), 129.0 (ArC), 136.1 (ArC), 146.3 (ArC), 147.6 (ArC), 156.8 (C14), 180.5 (C9).

IR (ATR, cm^{-1}): 3032, 2976, 2856, 1723, 1453, 1385, 1260, 1144, 726.

HRMS (ESI$^+$): Exact mass calculated for $C_{20}H_{21}N_2O_2^+$ (M + H^+) 321.1598. Found: 321.1598.

4.1.29. Synthesis of 2-(3-(2-ethoxypyridin-3-yl)phenyl)-2-methylpropanoic acid (31)

Prepared following the general procedure using **20** (140 mg, 0.487 mmol, 1.0 eq.) and sodium hydroxide (97 mg, 2.437 mmol, 5.0 eq.). Following work-up, **31** was recovered as a brown solid (120 mg, 0.420 mmol, 86 %).

^{1}H NMR (400 MHz, $CDCl_3$): δ 1.36 (3H, t, $J = 7.0$ Hz, H10), 1.65 (6H, s, H7), 4.40 (2H, q, $J = 7.2$ Hz, H11), 6.95 (1H, dd, $J = 7.2$ Hz, 4.6 Hz, H14), 7.39–7.46 (3H, m, ArH), 7.63 (1H, dd, $J = 7.0$ Hz, 1.8 Hz, H15), 7.70 (1H, br s, H6), 8.15 (1H, dd, $J = 4.5$ Hz, 1.9 Hz, H13).

^{13}C NMR (100 MHz, $CDCl_3$): δ 14.5 (C10), 26.3 (C7), 46.3 (C8), 61.9 (C11), 116.9 (C14), 124.4 (ArC), 124.9 (C16), 127.1 (C2), 127.6 (C4), 128.2 (ArC), 136.8 (C1), 138.7 (C15), 143.6 (ArC), 145.6 (C13), 160.5 (C12), 182.5 (C9).

IR (ATR, cm^{-1}): 3053, 2929, 2839, 1698, 1585, 1434, 1382, 1247, 703.

HRMS (ESI$^+$): Exact mass calculated for $C_{17}H_{20}NO_3^+$ (M + H^+) 286.1438. Found: 286.1437.

4.1.30. Synthesis of 2-(3-(2-fluoropyridin-3-yl)phenyl)-2-methylpropanoic acid (32)

A solution of **20** (190 mg, 0.661 mmol, 1.0 eq.) in 15 % aqueous sodium hydroxide (4 mL) and dimethylformamide (1 mL) was heated to reflux at 100 °C for 24 h. After completion, the reaction mixture was quenched with water (15 mL) and extracted with diethyl ether (2 X 20 mL). The aqueous layer was acidified with 2 N hydrochloric acid and extracted with ethyl acetate (2 X 20 mL). The combined organic layer was washed with brine (20 mL) and dried over magnesium sulfate. The organic layer was concentrated under vacuum to afford **32** as a colorless oil (100 mg, 0.385 mmol, 58 %).

^{1}H NMR (600 MHz, DMSO-d_6): δ 1.52 (6H, s, H7), 7.43 (1H, m, H3), 7.47–7.50 (3 H, m, ArH), 7.55 (1H, s, H6), 8.12 (1H, dd, $J = 7.8$ Hz, 4.5 Hz, H13), 8.25 (1H, d, $J = 4.8$ Hz, H12), 12.44 (1H, br s, H10).

^{13}C NMR (75 MHz, Acetone-d_6): 26.0 (C7), 46.1 (C8), 122.2 (d, $^4J_{C\text{-}F} = 4.3$ Hz, C12), 123.6 (d, $^2J_{C\text{-}F} = 28.8$ Hz, C14), 125.8 (C3), 126.3 (d, $^4J_{C\text{-}F} = 2.7$ Hz, C6), 127.0 (d, $^4J_{C\text{-}F} = 3.3$ Hz, C2), 128.6 (C4), 134.0 (d, $^3J_{C\text{-}F} = 5.0$ Hz, C1), 141.1 (d, $^3J_{C\text{-}F} = 4.4$ Hz, C13), 145.4 (C5), 146.4 (d, $^3J_{C\text{-}F} = 15.2$ Hz, C11), 160.3 (d, $^1J_{C\text{-}F} = 237.0$ Hz, C10), 176.8 (C9).

^{19}F NMR (282 MHz, Acetone-d_6): δ −72.82 (s, C–F).

IR (ATR, cm^{-1}): 3255, 2919, 2851, 1603, 1423, 1363, 1245, 1149, 702.

HRMS (ESI$^+$): Exact mass calculated for $C_{15}H_{15}FNO_2^+$ (M + H^+) 260.1081. Found: 260.1081.

4.1.31. General procedure for the synthesis of substituted 3-nitro-4-chloro urea derivatives (33–41)

To a solution of the appropriate carboxylic acid (1.0 eq.) in

dichloromethane (5 mL), cooled to 0 °C, was added triethylamine (1.3 eq.). Ethylchloroformate (1.2 eq.) was added dropwise, and the reaction mixture was stirred at the same temperature for 1 h. Sodium azide (1.1 eq.) was added and the reaction mixture was stirred at room temperature for 18 h. After completion, the reaction mixture was filtered and the filtrate was concentrated under vacuum to afford the azide intermediate. The azide was then dissolved in toluene (5 mL) and heated to reflux for 2 h. The solvent was concentrated under vacuum to afford the isocyanate. The isocyanate intermediate was dissolved in tetrahydrofuran (5 mL), cooled to 0 °C and triethylamine (1.3 eq.) was added. After stirring the reaction mixture for 10 min, 3-nitro-4-chloroaniline (1.2 eq.) was added and the reaction mixture was stirred at room temperature for 18 h. After completion, the reaction mixture was diluted with water (20 mL) and extracted with ethyl acetate (2 X 25 mL). The combined organic layer was washed with brine (1 X 20 mL) and dried over magnesium sulfate. The organic layer was concentrated under vacuum to afford a residue which was purified by silica gel column chromatography using the stated eluent system.

4.1.32. Synthesis of ethyl 4-(3-(2-(3-(4-chloro-3-nitrophenyl)ureido) propan-2-yl)phenyl)-1H-pyrazole-1-carboxylate (33)

Prepared following the general procedure using **24** (100 mg, 0.434 mmol, 1.0 eq.), ethylchloroformate (0.05 mL, 0.521 mmol, 1.2 eq.), triethylamine (0.08 mL, 0.564 mmol, 1.3 eq.) and sodium azide (31 mg, 0.477 mmol, 1.1 eq.). The resulting yellow colored oil was dissolved in toluene and heated to reflux for 2 h. The isocyanate intermediate (97 mg, 0.426 mmol, 1.0 eq.) was obtained as a yellow colored oil and was treated with 3-nitro-4-chloroaniline (88 mg, 0.512 mmol, 1.2 eq.) and triethylamine (0.08 mL, 0.554 mmol, 1.3 eq.) in tetrahydrofuran. The residue was purified by silica gel column chromatography using methanol-dichloromethane (0 %–5 %) to afford **33** as a yellow solid (25 mg, 0.052 mmol, 12 %).

^{1}H NMR (400 MHz, $CDCl_3$): δ 1.49 (3H, t, $J = 7.0$ Hz, H20), 1.72 (6H, s, H7), 4.56 (2H, q, $J = 7.2$ Hz, H19), 6.36 (1H, s, H9), 7.15 (1H, d, $J = 8.8$ Hz, H4), 7.32–7.42 (4H, m, ArH), 7.62 (2H, d, $J = 4.9$ Hz, H21, H23), 8.06 (1H, br s, H6), 8.09 (1H, br s, H11), 8.21 (1H, s, H13).

^{13}C NMR (100 MHz, $CDCl_3$): δ 14.2 (C20), 29.7 (C7), 55.1 (C8), 65.3 (C19), 114.5 (ArC), 118.4 (C13), 122.5 (ArC), 122.7 (ArC), 124.4 (C15), 124.5 (ArC), 126.4 (C23), 126.7 (C22), 129.3 (C21), 130.4 (ArC), 131.6 (C12), 139.3 (C1), 142.7 (ArC), 147.2 (C5), 148.6 (C14), 149.4 (C18), 154.2 (C10).

IR (ATR, cm^{-1}): 3355, 2925, 2881, 1754, 1661, 1590, 1530, 1381, 1260, 821, 700.

HRMS (ESI$^+$): Exact mass calculated for $C_{22}H_{23}^{35}ClN_5O_5^+$ ($M + H^+$) 472.1382. Found: 472.1377.

Melting Point: 120–123 °C.

HPLC Purity: 98.1 %

4.1.33. Synthesis of ethyl 3-(3-(2-(3-(4-chloro-3-nitrophenyl)ureido) propan-2-yl)phenyl)-1H-pyrazole-1-carboxylate (34)

Prepared following the general procedure using **25** (112 mg, 0.486 mmol, 1.0 eq.), ethylchloroformate (0.05 mL, 0.583 mmol, 1.2 eq.), triethylamine (0.09 mL, 0.632 mmol, 1.3 eq.) and sodium azide (35 mg, 0.535 mmol, 1.1 eq.). The resulting yellow colored oil was dissolved in toluene and heated to reflux for 2 h. The isocyanate intermediate (135 mg, 0.486 mmol, 1.0 eq.) was obtained as a yellow oil and was treated with 3-nitro-4-chloroaniline (100 mg, 0.584 mmol, 1.2 eq.) and triethylamine (0.09 mL, 0.623 mmol, 1.3 eq.) in tetrahydrofuran. The residue was purified by silica gel column chromatography using methanol-dichloromethane (0 %–5 %) to afford **34** as an off-white solid (70 mg, 0.148 mmol, 30 %).

^{1}H NMR (400 MHz, DMSO-d_6): δ 1.36 (3H, t, $J = 7.1$ Hz, H20), 1.66 (6H, s, H7), 4.46 (2H, q, $J = 7.1$ Hz, H19), 6.94 (1H, s, H9), 7.09 (1H, d, $J = 2.7$ Hz, H22), 7.40–7.48 (3H, m, ArH), 7.56 (1H, d, $J = 8.9$ Hz, H16), 7.74 (1H, d, $J = 7.4$ Hz, H2), 7.94 (1H, s, H6), 8.19 (1H, d, $J = 2.3$ Hz, H13), 8.39 (1H, d, $J = 2.6$ Hz, H21), 9.05 (1H, s, H11).

^{13}C NMR (100 MHz, $CDCl_3$): δ 14.0 (C20), 29.5 (C7), 55.3 (C8), 65.0 (C19), 107.6 (C22), 114.5 (ArC), 118.1 (C13), 122.4 (C15), 122.7 (ArC), 125.4 (ArC), 125.9 (ArC), 128.9 (ArC), 131.4 (ArC), 131.5 (C21), 132.3 (C12), 139.4 (C1), 147.4 (C5), 148.1 (C14), 149.4 (C18), 154.3 (C23), 156.6 (C10).

IR (ATR, cm^{-1}): 3353, 2929, 1756, 1661, 1590, 1536, 1385, 1283, 1245, 822.

HRMS (ESI$^+$): Exact mass calculated for $C_{22}H_{23}^{35}ClN_5O_5^+$ ($M + H^+$) 472.1382. Found: 472.1381.

Melting Point: 98–101 °C.

HPLC Purity: 95.4 %

4.1.34. Synthesis of 1-(4-chloro-3-nitrophenyl)-3-(2-(3-(thiophen-2-yl) phenyl)propan-2-yl)urea (35)

Prepared following the general procedure using **26** (143 mg, 0.580 mmol, 1.0 eq.), ethylchloroformate (0.07 mL, 0.696 mmol, 1.2 eq.), triethylamine (0.10 mL, 0.754 mmol, 1.3 eq.) and sodium azide (41 mg, 0.638 mmol, 1.1 eq.). The resulting brown oil was dissolved in toluene and heated to reflux for 2 h. The isocyanate intermediate (140 mg, 0.575 mmol, 1.0 eq.) was obtained as a brown colored oil and was treated with 3-nitro-4-chloroaniline (118 mg, 0.690 mmol, 1.2 eq.) and triethylamine (0.1 mL, 0.747 mmol, 1.3 eq.) in tetrahydrofuran. The residue was purified by silica gel column chromatography using ethyl acetate-hexane (0 %–20 %) to afford **35** as a green solid (60 mg, 0.144 mmol, 25 %).

^{1}H NMR (400 MHz, $CDCl_3$): δ 1.55 (6H, s, H7), 6.85 (1H, s, H9), 7.05 (1H, app. t, $J = 4.3$ Hz, H19), 7.21–7.27 (5H, m, ArH), 7.35 (1H, d, $J = 4.4$ Hz, H18), 7.48 (1H, d, $J = 4.3$ Hz, H20), 7.66 (1H, br s, H6), 7.72 (1H, br s, H13).

^{13}C NMR (100 MHz, $CDCl_3$): δ 29.7 (C7), 55.1 (C8), 115.0 (ArC), 119.2 (C13), 122.1 (ArC), 123.1 (ArC), 123.2 (ArC), 123.8 (C15), 124.3 (ArC), 124.9 (C18), 128.0 (C19), 129.2 (C20), 131.6 (ArC), 134.5 (C1), 138.6 (C12), 144.0 (C21), 147.3 (C5), 147.7 (C14), 154.5 (C10).

IR (ATR, cm^{-1}): 3330, 2976, 2825, 1651, 1531, 854, 820, 697.

HRMS (ESI$^+$): Exact mass calculated for $C_{20}H_{19}^{35}ClN_3O_3S^+$ ($M + H^+$) 416.0830. Found: 416.0817.

Melting Point: 84–87 °C.

HPLC Purity: 95.3 %

4.1.35. Synthesis of 1-(4-chloro-3-nitrophenyl)-3-(2-(3-(furan-2-yl) phenyl)propan-2-yl)urea (36)

Prepared following the general procedure using **27** (110 mg, 0.477 mmol, 1.0 eq.), ethylchloroformate (0.05 mL, 0.573 mmol, 1.2 eq.), triethylamine (0.08 mL, 0.621 mmol, 1.3 eq.) and sodium azide (34 mg, 0.525 mmol, 1.1 eq.). The resulting yellow colored oil was dissolved in toluene and heated to reflux for 2 h. The isocyanate intermediate (108 mg, 0.475 mmol, 1.0 eq.) was obtained as a brown colored oil and was treated with 3-nitro-4-chloroaniline (98 mg, 0.570 mmol, 1.2 eq.) and triethylamine (0.09 mL, 0.617 mmol, 1.3 eq.) in tetrahydrofuran. The residue was purified by silica gel column chromatography using ethyl acetate-hexane (0 %–20 %) to afford **36** as a yellow solid (25 mg, 0.062 mmol, 13 %).

^{1}H NMR (300 MHz, $CDCl_3$): δ 1.58 (6H, s, H7), 5.87 (1H, s, H9), 6.40 (1H, dd, $J = 3.3$ Hz, 1.8 Hz, H19), 6.54 (1H, d, $J = 3.1$ Hz, H18), 6.89 (1H, dd, $J = 8.7$ Hz, 2.3 Hz, H17), 7.14 (1H, d, $J = 8.6$ Hz, H16), 7.21–7.44 (5H, m, ArH), 7.68 (1H, s, H6), 7.82 (1H, d, $J = 2.4$ Hz, H13).

^{13}C NMR (100 MHz, $CDCl_3$): δ 29.6 (C7), 55.0 (C8), 105.2 (C18), 111.7 (C19), 119.1 (ArC), 119.7 (C13), 122.1 (ArC), 123.0 (ArC), 123.6 (C15), 128.9 (C1), 131.0 (ArC), 131.6 (ArC), 138.5 (C12), 142.0 (C20), 147.3 (C5), 147.6 (C14), 153.5 (C21), 154.7 (C10).

IR (ATR, cm^{-1}): 3333, 2927, 1652, 1531, 1384, 1168, 819, 733.

HRMS (ESI$^+$): Exact mass calculated for $C_{20}H_{18}^{35}ClN_3O_4Na^+$ ($M + Na^+$) 422.0878. Found: 422.0891.

Melting Point: 92–95 °C.

HPLC Purity: 97.6 %

4.1.36. Synthesis of 1-(4-chloro-3-nitrophenyl)-3-(2-(3-(thiazol-2-yl) phenyl)propan-2-yl)urea (37)

Prepared following the general procedure using **28** (110 mg, 0.444 mmol, 1.0 eq.), ethylchloroformate (0.05 mL, 0.533 mmol, 1.2 eq.), triethylamine (0.08 mL, 0.578 mmol, 1.3 eq.) and sodium azide (32 mg, 0.489 mmol, 1.1 eq.). The resulting yellow colored oil was dissolved in toluene and heated to reflux for 2 h. The isocyanate intermediate (108 mg, 0.442 mmol, 1.0 eq.) was obtained as a yellow colored oil and was treated with 3-nitro-4-chloroaniline (91 mg, 0.530 mmol, 1.2 eq.) and triethylamine (0.08 mL, 0.574 mmol, 1.3 eq.) in tetrahydrofuran. The residue was purified by silica gel column chromatography using ethyl acetate-hexane (0 %–40 %) to afford **37** as a brown solid (60 mg, 0.143 mmol, 32 %).

^{1}H NMR (400 MHz, $CDCl_3$): δ 1.55 (6H, s, H7), 6.30 (1H, s, H9), 6.88 (1H, dd, J = 8.7 Hz, 2.3 Hz, H17), 7.09 (1H, d, J = 8.6 Hz, H16), 7.29 (1H, d, J = 3.2 Hz, H19), 7.32–7.40 (2H, m, ArH), 7.64 (1H, d, J = 7.1 Hz, H2), 7.76 (1H, d, J = 3.1 Hz, H18), 7.82 (1H, d, J = 2.3 Hz, H13), 8.01 (1H, br s, H6), 8.05 (1H, br s, H11).

^{13}C NMR (100 MHz, $CDCl_3$): δ 29.7 (C7), 55.1 (C8), 114.6 (ArC), 118.8 (C19), 119.5 (C13), 122.5 (ArC), 122.7 (C15), 125.3 (ArC), 126.9 (ArC), 129.4 (ArC), 131.6 (ArC), 132.8 (C1), 138.8 (C12), 142.6 (C5), 147.4 (C18), 148.5 (C14), 154.4 (C10), 168.9 (C20).

IR (ATR, cm^{-1}): 3332, 2923, 2860, 1655, 1592, 1532, 1480, 1384, 1168, 735.

HRMS (ESI$^+$): Exact mass calculated for $C_{19}H_{18}^{35}ClN_4O_3S^+$ ($M + H^+$) 417.0783. Found: 417.0769.

Melting Point: 86–89 °C.

HPLC Purity: 99.2 %

4.1.37. Synthesis of 1-(4-chloro-3-nitrophenyl)-3-(2-(3-(1-trityl-1H-imidazole-4-yl)phenyl)propan-2-yl)urea (38)

Prepared following the general procedure using **29** (200 mg, 0.423 mmol, 1.0 eq.), ethylchloroformate (0.05 mL, 0.507 mmol, 1.2 eq.), triethylamine (0.08 mL, 0.550 mmol, 1.3 eq.) and sodium azide (30 mg, 0.465 mmol, 1.1 eq.). The resulting yellow colored oil was dissolved in toluene and heated to reflux for 2 h. The isocyanate intermediate (195 mg, 0.415 mmol, 1.0 eq.) was obtained as a brown colored oil and was treated with 3-nitro-4-chloroaniline (85 mg, 0.498 mmol, 1.2 eq.) and triethylamine (0.07 mL, 0.539 mmol, 1.3 eq.) in tetrahydrofuran. The residue was purified by silica gel column chromatography using ethyl acetate-hexane (0 %–50 %) to afford **38** as a white solid (125 mg, 0.194 mmol, 46 %).

^{1}H NMR (400 MHz, $CDCl_3$): δ 1.60 (6H, s, H7), 6.65 (1H, s, H9), 7.00–7.06 (2H, m, ArH), 7.16–7.21 (8H, m, ArH), 7.35–7.36 (11H, m, ArH), 7.49 (1H, br s, H6), 7.75 (1H, d, J = 1.8 Hz, H20), 8.18 (1H, s, H13), 8.65 (1H, s, H11).

^{13}C NMR (150 MHz, DMSO-d_6): δ 29.9 (C7), 55.0 (C8), 75.2 (C21), 113.6 (ArC), 116.0 (C13), 117.8 (C19), 121.2 (ArC), 122.6 (ArC), 122.9 (ArC), 123.6 (C15), 128.4 (ArC), 128.6 (ArC), 128.7 (ArC), 129.6 (ArC), 132.0 (C1), 134.1 (ArC), 139.0 (C20), 140.8 (ArC), 140.9 (C18), 142.6 (ArC), 147.9 (C14), 148.6 (C5), 153.9 (C10).

IR (ATR, cm^{-1}): 3332, 2924, 2854, 1667, 1595, 1536, 1484, 1361, 1284, 745.

HRMS (ESI$^+$): Exact mass calculated for $C_{38}H_{33}^{35}ClN_5O_3^+$ ($M + H^+$) 642.2266. Found: 642.2264.

Melting Point: 236–239 °C.

HPLC Purity: 99.6 %

4.1.38. Synthesis of 1-(2-(3-(1-benzyl-1H-imidazole-2-yl)phenyl)propan-2-yl)-3-(4-chloro-3-nitrophenyl)urea (39)

Prepared following the general procedure using **30** (50 mg, 0.156 mmol, 1.0 eq.), ethylchloroformate (0.02 mL, 0.187 mmol, 1.2 eq.), triethylamine (0.03 mL, 0.203 mmol, 1.3 eq.) and sodium azide (11 mg, 0.171 mmol, 1.1 eq.). The resulting brown colored oil was dissolved in toluene and heated to reflux for 2 h. The isocyanate intermediate (45 mg, 0.141 mmol, 1.0 eq.) was obtained as a brown colored oil and was treated with 3-nitro-4-chloroaniline (29 mg, 0.169 mmol, 1.2 eq.) and triethylamine (0.02 mL, 0.184 mmol, 1.3 eq.) in tetrahydrofuran. The residue was purified by silica gel column chromatography using ethyl acetate-hexane (0 %–50 %) to afford **39** as a yellow solid (45 mg, 0.091 mmol, 59 %).

^{1}H NMR (600 MHz, DMSO-d_6): δ 1.53 (6H, s, H7), 5.25 (2H, s, H20), 6.87 (1H, s, H9), 6.95 (2H, d, J = 7.0 Hz, ArH), 7.03 (1H, br s, ArH), 7.21 (1H, d, J = 7.2 Hz, H4), 7.24–7.28 (3H, m, ArH), 7.37 (2H, d, J = 7.3 Hz, ArH), 7.38 (1H, d, J = 2.5 Hz, H18), 7.40 (1H, d, J = 2.5 Hz, H19), 7.43 (1H, d app. t, J = 7.1 Hz, 1.8 Hz, ArH), 7.53 (2H, d, J = 7.8 Hz, ArH), 8.17 (1H, d, J = 2.5 Hz, H13), 9.00 (1H, s, H11).

^{13}C NMR (100 MHz, DMSO-d_6): δ 29.8 (C7), 50.0 (C20), 54.9 (C8), 113.6 (ArC), 116.1 (C13), 122.6 (C19), 122.8 (C15), 125.3 (ArC), 125.5 (ArC), 126.5 (ArC), 126.9 (ArC), 127.8 (C18), 128.5 (C12), 128.8 (ArC), 129.0 (ArC), 129.1 (ArC), 130.7 (ArC), 132.0 (C1), 138.0 (ArC), 140.8 (ArC), 147.5 (C5), 147.8 (C14), 148.9 (C10), 153.9 (C21).

IR (ATR, cm^{-1}): 3328, 2922, 2854, 1708, 1598, 1533, 1454, 1360, 1282, 725, 704.

HRMS (ESI$^+$): Exact mass calculated for $C_{26}H_{25}^{35}ClN_5O_3^+$ ($M + H^+$) 490.1640. Found: 490.1627.

Melting Point: 208–211 °C.

HPLC Purity: 95.4 %

4.1.39. Synthesis of 1-(4-chloro-3-nitrophenyl)-3-(2-(3-(2-ethoxypyridin-3-yl)phenyl)propan-2-yl)urea (40)

Prepared following the general procedure using **31** (95 mg, 0.332 mmol, 1.0 eq.), ethylchloroformate (0.04 mL, 0.399 mmol, 1.2 eq.), triethylamine (0.06 mL, 0.432 mmol, 1.3 eq.) and sodium azide (23 mg, 0.366 mmol, 1.1 eq.). The resulting yellow colored oil was dissolved in toluene and heated to reflux for 2 h. The isocyanate intermediate (90 mg, 0.318 mmol, 1.0 eq.) was obtained as a brown colored oil and was treated with 3-nitro-4-chloroaniline (65 mg, 0.382 mmol, 1.2 eq.) and triethylamine (0.06 mL, 0.414 mmol, 1.3 eq.) in tetrahydrofuran. The residue was purified by silica gel column chromatography using ethyl acetate-hexane (0 %–30 %) to afford **40** as a yellow solid (30 mg, 0.065 mmol, 20 %).

^{1}H NMR (400 MHz, $CDCl_3$): δ 1.27 (3H, t, J = 6.0 Hz, H18), 1.60 (6H, s, H7), 4.32 (2H, q, J = 6.7 Hz, H19), 6.22 (1H, s, H9), 6.88 (1H, app. t, J = 6.6 Hz, H22), 6.98 (1H, d, J = 7.7 Hz, H4), 7.12 (1H, d, J = 8.4 Hz, H16), 7.30–7.34 (4H, m, ArH), 7.49 (1H, d, J = 6.7 Hz, H21), 7.67 (1H, s, H6), 7.93 (1H, br s, H13), 8.04 (1H, br s, H11).

^{13}C NMR (100 MHz, $CDCl_3$): δ 14.6 (C18), 29.9 (C7), 55.3 (C8), 62.1 (C19), 114.7 (ArC), 117.1 (C22), 119.0 (C13), 122.8 (ArC), 123.9 (C15), 124.2 (ArC), 125.8 (C24), 127.5 (ArC), 128.5 (ArC), 131.7 (C23), 136.7 (C1), 138.8 (C12), 145.3 (C5), 146.6 (C21), 147.4 (C14), 154.5 (C10), 160.1 (C20).

IR (ATR, cm^{-1}): 3343, 2975, 2854, 1658, 1586, 1534, 1434, 1382, 1248, 735.

HRMS (ESI$^+$): Exact mass calculated for $C_{23}H_{24}^{35}ClN_4O_4^+$ ($M + H^+$) 455.1481. Found: 455.1480.

Melting Point: 80–83 °C.

HPLC Purity: 99.5 %

4.1.40. Synthesis of 1-(4-chloro-3-nitrophenyl)-3-(2-(3-(2-fluoropyridin-3-yl)phenyl)propan-2-yl)urea (41)

Prepared following the general procedure using **32** (100 mg, 0.385 mmol, 1.0 eq.), ethylchloroformate (0.04 mL, 0.463 mmol, 1.2 eq.), triethylamine (0.07 mL, 0.501 mmol, 1.3 eq.) and sodium azide (27 mg, 0.424 mmol, 1.1 eq.). The resulting yellow colored oil was dissolved in toluene and heated to reflux for 2 h. The isocyanate intermediate (98 mg, 0.382 mmol, 1.0 eq.) was obtained as a brown colored oil and was treated with 3-nitro-4-chloroaniline (79 mg, 0.459 mmol, 1.2 eq.) and triethylamine (0.07 mL, 0.497 mmol, 1.3 eq.) in tetrahydrofuran. The residue was purified by silica gel column chromatography using ethyl acetate-hexane (0 %–50 %) to afford **41** as a brown solid (25 mg, 0.058 mmol, 15 %).

^{1}H NMR (600 MHz, Acetone-d_6): δ 1.61 (6H, s, H7), 6.41 (1H, s, H9), 7.26–7.35 (4H, m, ArH), 7.39–7.44 (2H, m, ArH), 7.60 (1H, br s, H6), 7.91 (1H, dd, J = 7.8 Hz, 1.9 Hz, H17), 8.06 (1H, d, J = 4.6 Hz, H19), 8.26 (1H, d, J = 2.0 Hz, H13), 8.48 (1H, br s, H11).

^{13}C NMR (150 MHz, Acetone-d_6): δ 29.3 (C7), 55.0 (C8), 113.7 (C13), 116.4 (C3), 122.1 (C15), 122.2 (d, $^4J_{C\text{-}F}$ = 3.9 Hz, C20), 123.8 (d, $^2J_{C\text{-}F}$ = 28.6 Hz, C22), 125.0 (C17), 125.5 (d, $^4J_{C\text{-}F}$ = 2.4 Hz, C6), 126.6 (d, $^4J_{C\text{-}F}$ = 2.6 Hz, C2), 128.5 (C4), 131.4 (C16), 133.7 (d, $^3J_{C\text{-}F}$ = 4.9 Hz, C1), 140.8 (C12), 141.0 (d, $^3J_{C\text{-}F}$ = 4.2 Hz, C21), 146.3 (d, $^3J_{C\text{-}F}$ = 15.7 Hz, C19), 148.2 (C5), 148.8 (C14), 153.5 (C10), 160.3 (d, $^1J_{C\text{-}F}$ = 238.3 Hz, C18).

^{19}F NMR (376 MHz, Acetone-d_6): δ −71.37 (s, C–F).

IR (ATR, cm^{-1}): 3341, 2926, 2856, 1657, 1596, 1534, 1389, 1248, 1169, 737.

HRMS (ESI$^+$): Exact mass calculated for $C_{21}H_{19}^{35}ClFN_4O_3^+$ (M + H$^+$) 429.1124. Found: 429.1111.

Melting Point: 69–72 °C.

HPLC Purity: 97.1 %

4.1.41. General procedure for the deprotection of pyrazoles 33 and 34

A solution of the appropriate protected pyrazole (1.0 eq.) and triethylamine (1.2 eq.) in methanol (5 mL) was stirred at room temperature for 18 h. After completion, the reaction mixture was concentrated under vacuum and the resulting residue was purified by silica gel column chromatography using the stated eluent system.

4.1.42. Synthesis of 1-(2-(3-(1H-pyrazol-4-yl)phenyl)propan-2-yl)-3-(4-chloro-3-nitrophenyl)urea (42)

Prepared following the general procedure using **33** (45 mg, 0.095 mmol, 1.0 eq.) and triethylamine (0.02 mL, 0.114 mmol, 1.2 eq.) The residue was purified by silica gel column chromatography using methanol-dichloromethane (0 %–3 %) to afford **42** as a yellow solid (25 mg, 0.062 mmol, 66 %).

^{1}H NMR (400 MHz, Acetone-d_6): δ 1.60 (6H, s, H7), 6.37 (1H, s, H9), 7.14–7.21 (2H, m, ArH), 7.30–7.34 (2H, m, ArH), 7.39 (1H, dd, J = 8.8 Hz, 2.5 Hz, H17), 7.60 (1H, s, H6), 7.88 (2H, br s, H18, H19), 8.14 (1H, d, J = 2.4 Hz, H13), 8.42 (1H, s, H11).

^{13}C NMR (100 MHz, CD_3OD): δ 30.2 (C7), 56.2 (C8), 79.5 (ArC), 115.3 (ArC), 118.6 (ArC), 123.3 (C15), 123.4 (ArC), 124.3 (ArC), 124.9 (C20), 129.9 (C18, C19), 132.7 (ArC), 133.5 (C12), 141.4 (ArC), 149.5 (C5), 149.7 (C14), 155.9 (C10).

IR (ATR, cm^{-1}): 3316, 2927, 2854, 1659, 1591, 1530, 1383, 1249, 821, 701.

HRMS (ESI$^+$): Exact mass calculated for $C_{19}H_{19}^{35}ClN_5O_3^+$ (M + H$^+$) 400.1170. Found: 400.1178.

Melting Point: 130–133 °C.

HPLC Purity: 97.1 %

4.1.43. Synthesis of 1-(2-(3-(1H-pyrazol-3-yl)phenyl)propan-2-yl)-3-(4-chloro-3-nitrophenyl)urea (43)

Prepared following the general procedure using **34** (40 mg, 0.084 mmol, 1.0 eq.) and triethylamine (0.01 mL, 0.114 mmol, 1.2 eq.). The residue was purified by silica gel column chromatography using methanol-dichloromethane (0 %–3 %) to afford **43** as a yellow solid (27 mg, 0.067 mmol, 82 %).

^{1}H NMR (400 MHz, DMSO-d_6): δ 1.65 (6H, s, H7), 6.68 (1H, s, H9), 6.89 (1H, br s, H20), 7.34–7.45 (3H, m, ArH), 7.55–7.70 (3H, m, ArH), 7.84 (1H, br s, H6), 8.20 (1H, s, H13), 8.31 (1H, br s, H11), 9.05 (1H, s, H18).

^{13}C NMR (100 MHz, CD_3OD): δ 29.4 (C7), 54.5 (C8), 79.1 (ArC), 101.9 (C20), 113.1 (ArC), 115.3 (C13), 121.6 (ArC), 122.1 (ArC), 123.1 (C15), 123.9 (ArC), 128.3 (ArC), 131.5 (C19), 140.5 (ArC), 147.4 (C5), 148.4 (C14), 149.5 (C21), 153.5 (C10).

IR (ATR, cm^{-1}): 3320, 2928, 2854, 1658, 1590, 1531, 1384, 1248, 821, 700.

HRMS (ESI$^+$): Exact mass calculated for $C_{19}H_{19}^{35}ClN_5O_3^+$ (M + H$^+$) 400.1170. Found: 400.1167.

Melting Point: 124–126 °C.

HPLC Purity: 99.1 %

4.1.44. Synthesis of 1-(2-(3-(1H-imidazole-4-yl)phenyl)propan-2-yl)-3-(4-chloro-3-nitrophenyl)urea (44)

A solution of **38** (125 mg, 0.194 mmol, 1.0 eq.) and acetic acid (0.5 mL) in methanol (5 mL) was stirred at room temperature for 24 h. After completion, the reaction mixture was concentrated under vacuum and the resulting residue was purified by silica gel column chromatography using methanol-dichloromethane (0 %–4 %) to afford **44** as an off-white solid (18 mg, 0.045 mmol, 23 %).

^{1}H NMR (600 MHz, CD_3OD): δ 1.72 (6H, s, H7), 7.32–7.37 (2H, m, ArH), 7.41–7.46 (3H, m, ArH), 7.53 (1H, d, J = 7.1 Hz, H2), 7.82 (2H, br s, H19, H20), 7.89 (1H, s, H6), 8.03 (1H, d, J = 2.0 Hz, H13).

^{13}C NMR (125 MHz, CD_3OD): δ 30.1 (C7), 56.2 (C8), 115.3 (C13), 118.6 (C19), 122.6 (ArC), 123.4 (C15), 124.1 (ArC), 124.7 (ArC), 129.7 (ArC), 132.6 (ArC), 133.7 (C20), 141.3 (C18), 149.5 (ArC), 149.6 (C14), 155.9 (C10).

IR (ATR, cm^{-1}): 3323, 2918, 2849, 1672, 1537, 1463, 1385, 1259, 1032, 751.

HRMS (ESI$^+$): Exact mass calculated for $C_{19}H_{19}^{35}ClN_5O_3^+$ (M + H$^+$) 400.1170. Found: 400.1179.

Melting Point: 150–152 °C.

HPLC Purity: 96.6 %

4.2. Biological evaluation

4.2.1. Expression and purification of IMPDH variants

All recombinant proteins were expressed in *E. coli* BL21 (DE3)/pDIA17 strains as fusion proteins with a His-tag at the N-terminus part, except for hIMPDH2 which was purchased from NOVOCIB SAS (France). The proteins were purified using a two-steps procedure, as described previously [32,41,42]. Briefly, a first purification by affinity chromatography was performed using a TALON metal affinity resin (TaKaRa Bio USA, Inc.) and followed by size exclusion chromatography using a HiLoad™ 26/60 Superdex™ 200 prep grade (Cytiva Life Sciences) previously equilibrated with the corresponding purification buffer (see Table 8) supplemented with 1 mM DTT and 1 mM EDTA.

4.2.2. Enzymatic assays and kinetic characterization of IMPDH variants

Enzymatic assays for each IMPDH variant were performed at 30 °C, by monitoring the formation of NADH at 340 nm in the corresponding optimal kinetic buffer (see Table 8) at various concentrations of IMP, NAD^+, ATP, $MgCl_2$ and compounds identified herein, using an Eppendorf ECOM 6122 photometer. Concerning hIMPDH2, the enzymatic

Table 8
Composition of purification and kinetic buffers for each IMPDH variant.

Protein	Protein description	Purification buffer	Kinetics buffer
IMPDHec	*E. coli* IMPDH WT	Tris-HCl 50 mM pH 9 KCl 100 mM	Tris-HCl 50 mM pH 8 KCl 50 mM
IMPDHec-ΔDB	*E. coli* BD-deleted IMPDH variant		Tris-HCl 50 mM pH 9 KCl 100 mM
IMPDHpa	*P. aeruginosa* IMPDH WT	K_2HPO_4 50 mM pH 8 KCl 100 mM	Tris-HCl 50 mM pH 8 KCl 100 mM
IMPDHpa-ΔDB	*P. aeruginosa* BD-deleted IMPDH variant		
IMPDHsa	*S. aureus* IMPDH WT	K_2HPO_4 50 mM pH 8 KCl 50 mM	Na_2CO_3 50 mM pH 9.2 KCl 20 mM
hIMPDH2	Isoform 2 of human IMPDH	–	Tris-HCl 100 mM pH 9 KCl 100 mM, DTT 5 mM

assays were performed according to the manufacturer's recommendations, using 1 mM IMP and 0.5 mM NAD^+ at 37 °C.

Data of at least three individual experiments were fitted using GraphPad Prim (Synergy Software, Inc.) and KaleidaGraph (Synergy Software, Inc.) according to the dose response logistic for the determination of I_{50} values and to the Michaelis–Menten equation for the determination of the mode of inhibition.

4.2.3. Enzymatic assay on TMP kinase from M. tuberculosis

The expression and purification of TMP kinase from *M. tuberculosis* were performed as described previously [45]. TMP kinase activity was determined at 30 °C by monitoring the consumption of NADH using the coupled spectrophotometric assay [53] at 340 nm in an Eppendorf ECOM 6122 photometer. The reaction medium (0.5 mL final volume) contained 50 mM Tris-HCl pH 7.4, 50 mM KCl, 2 mM $MgCl_2$, 0.2 mM NADH, 1 mM phosphoenol pyruvate, and 2 units each of lactate dehydrogenase, pyruvate kinase, and nucleoside diphosphate kinase. The concentrations of ATP and dTMP were kept constant at 0.5 and 0.05 mM, respectively.

4.2.4. 3D modelling and docking studies

Three-dimensional modelling was performed as previously described with slight modifications [54,55]. Briefly, sequence alignments between IMPDH and templates (pdb: 1ZFJ, 5AHL, 6U8S) were generated using Clustal W [56] and were manually refined. Three-dimensional IMPDH models were built from these alignments and crystallographic atomic coordinates of templates using the automated comparative modeling tool MODELER (Sali and Blundell) implemented in Discovery Studio. The best models selected based on the DOPE score (Discrete Optimized Protein Energy) and potential energy calculated by modeler, were solvated in a 10 Å water box with 0.145 M NaCl and minimized using Adopted Basis NR algorithm to a final gradient of 0.001. Hydrophobic properties and the volume of the binding site were predicted using Discovery Studio's embedded algorithm.

Flexible ligand-rigid protein docking was performed using CDOCKER, implemented in Discovery Studio 2020 [57]. Random ligand conformations were generated from the initial ligand structure through high-temperature molecular dynamics. The best poses, determined by their scores [58] were retained and clustered according to their binding modes.

4.2.5. Caco-2 cell culture and treatments

The Caco-2 cell line, derived from a human colon adenocarcinoma, is commonly used for toxicity assays. Caco-2 cells were cultured in Dulbecco's modified Eagle's essential medium (DMEM, Gibco 41965) containing 25 mM glucose and supplemented with 10 % fetal bovine serum (FBS), 1 % penicillin–streptomycin and 1 % non-essential amino acids. Cells were maintained at 37 °C in a humidified atmosphere with 5 % CO_2. For maintenance, pre-confluent cells were detached using trypsin/EDTA and seeded into new flask, with the medium changed every 2 days. For treatments, Caco-2 cells were seeded at a density of 1.10^5 cells/cm^2 in 96-well plates to reach confluency after 48h. Confluent cells were then exposed to compounds **42**, **43** and **44** at concentrations of 1 μM or 10 μM for 72h. DMSO at 0.1 % was used as vehicle of compounds and 0.2 % Triton X-100 was used as positive control of cytotoxicity.

4.2.6. Cellular toxicity evaluation

Cellular toxicity of compounds **42**, **43** and **44** was assessed by measuring cell viability and cell death of Caco-2 cells after 72h of exposure. Cell viability was determined using the Alamar Blue assay (Invitrogen, DAL1025), and cell death was evaluated by staining with propidium iodide (PI) and Hoechst 33342. Alamar Blue is a resazurin-based dye that is converted to fluorescent resorufin by dehydrogenases in living cells. Hoechst is a cell-membrane permeant nucleic acid stain that allows cell number assessment. PI is a nuclear dye that penetrates the cell membranes of dying cells, but is excluded from viable cells.

After exposure to compounds **42**, **43** and **44,** cells were rinsed twice with Phosphate Buffered Saline (PBS) buffer and incubated in FBS-free medium supplemented with 5 % Alamar Blue solution or 10 μg/mL PI and 10 μg/mL Hoechst solution for 30 min at 37 °C. Fluorometric quantifications were then measured using a plate reader (Tecan Infinite M1000 Pro). The excitation and emission wavelengths were 530 nm and 570 nm, respectively, for Alamar Blue; 535 nm and 617 nm, respectively, for PI; and 361 nm and 486 nm, respectively for Hoechst. Cell viability was expressed as resorufin fluorescence relative/compared to DMSO, and cell death was expressed as the ratio of PI fluorescence to Hoechst fluorescence relative to DMSO.

4.2.7. Antimicrobial growth inhibition assays

Antimicrobial evaluation against *S. aureus* (ATCC 43300) was undertaken at the Community for Open Antimicrobial Drug Discovery at The University of Queensland (Australia) according to their standard protocols [59].

CRediT authorship contribution statement

Nour Ayoub: Writing – original draft, Methodology, Investigation, Formal analysis, Data curation. **Amit Upadhyay:** Writing – original draft, Methodology, Investigation, Data curation. **Arnaud Tête:** Writing – original draft, Visualization, Software, Formal analysis. **Nicolas Pietrancosta:** Writing – original draft, Visualization, Software, Formal analysis. **Hélène Munier-Lehmann:** Writing – review & editing, Writing – original draft, Supervision, Resources, Funding acquisition, Conceptualization. **Timothy P. O'Sullivan:** Writing – review & editing, Writing – original draft, Supervision, Funding acquisition, Conceptualization.

Declaration of competing interest

The authors declare that they have no known competing financial interests or personal relationships that could have appeared to influence the work reported in this paper.

Data availability

Data is provided in the Supplementary Information

Acknowledgements

Amit Upadhyay is grateful for funding by way of a Government of Ireland Postgraduate Research Scholarship (GOIPG/2019/1117) provided by the Irish Research Council. This work was undertaken using equipment provided by Science Foundation Ireland though a research infrastructure award for process flow spectroscopy (ProSpect) (SFI 15/RI/3221). Nour Ayoub acknowledges a PhD fellowship from Médicament, Toxicologie, Chimie et Imagerie PhD school (MTCI, ED 563), Université Paris Cité. Some of the antimicrobial screening was performed by CO-ADD (The Community for Antimicrobial Drug Discovery), funded by the Wellcome Trust (UK) and The University of Queensland (Australia).

Appendix A. Supplementary data

Supplementary data to this article can be found online at https://doi.org/10.1016/j.ejmech.2024.116920.

Abbreviations

AMR	Antimicrobial resistance
ATR	Attenuated Total Reflectance
BD	Bateman domain

DCC	*N,N′*-Dicyclohexylcarbodiimide
dba	Dibenzylideneacetone
dGTP	2′-Deoxyguanosine-5′-triphosphate
DMEM	Dubelcco's modified Eagle's medium
DMF	Dimethylformamide
DMSO	Dimethyl sulfoxide
DNA	Deoxyribonucleic acid
DTT	Dithiothreitol
EDTA	Ethylenediaminetetraacetic acid
ESKAPEE	*Enterococcus faecium*, *Staphylococcus aureus*, *Klebsiella pneumoniae*, *Acinetobacter baumannii*, *Pseudomonas aeruginosa*, *Enterobacter* species and *Escherichia coli*
FBS	Fetal bovine serum
GMP	Guanosine 5′-monophosphate
GTP	Guanosine 5′-triphosphate
HRMS	High-resolution mass spectrometry
IMP	Inosine 5′-monophosphate
IMPDH	Inosine 5′-monophosphate dehydrogenase
IMPDHec	IMPDH from *E. coli*
IMPDHpa	IMPDH from *P. aeruginosa*
IMPDHsa	IMPDH from *S. aureus*
IMPDH ΔBD	IMPDH variant lacking the Bateman domain
I_{50}	The concentration of inhibitor required to produce 50 % inhibition of an enzymatic reaction at a specific substrate concentration
IR	Infra-red
MRSA	Methicillin-resistant *S. aureus*
MW	Microwave
NAD	Nicotinamide adenine dinucleotide
ND	Not determined
PI	Propidium iodide
RNA	Ribonucleic acid
SAR	Structure activity relationship
TMP	Thymidine monophosphate
XMP	Xanthosine-5′-monophosphate

References

[1] C.J. Murray, K.S. Ikuta, F. Sharara, L. Swetschinski, G.R. Aguilar, A. Gray, C. Han, C. Bisignano, P. Rao, E. Wool, Global burden of bacterial antimicrobial resistance in 2019: a systematic analysis, Lancet 399 (2022) 629–655.

[2] B. Jonas Olga, I. Alec, B.F.C. Jean, G. Le Gall Francois, V. Marquez Patricio, Drug-resistant Infections: a Threat to Our Economic Future (Vol. 2): Final Report (English). HNP/Agriculture Global Antimicrobial Resistance Initiative, World Bank Group, Washington, DC, 2021.

[3] S.C. Roberts, T.R. Zembower, Global increases in antibiotic consumption: a concerning trend for WHO targets, Lancet Infect. Dis. 21 (2021) 10–11.

[4] N. Bednarčuk, A. Golić Jelić, S. Stoisavljević Šatara, N. Stojaković, V. Marković Peković, M.P. Stojiljković, N. Popović, R. Škrbić, Antibiotic utilization during COVID-19: are we over-prescribing? Antibiotics 12 (2023) 308.

[5] M.S. Butler, I.R. Henderson, R.J. Capon, M.A. Blaskovich, Antibiotics in the clinical pipeline as of December 2022, J. Antibiot. 76 (2023) 431–473.

[6] L. Serwecińska, Antimicrobials and antibiotic-resistant bacteria: a risk to the environment and to public health, Water 12 (2020) 3313.

[7] D. Chinemerem Nwobodo, M.C. Ugwu, C. Oliseloke Anie, M.T. Al-Ouqaili, J. Chinedu Ikem, U. Victor Chigozie, M. Saki, Antibiotic resistance: the challenges and some emerging strategies for tackling a global menace, J. Clin. Lab. Anal. 36 (2022) e24655.

[8] E.M. Darby, E. Trampari, P. Siasat, M.S. Gaya, I. Alav, M.A. Webber, J.M. Blair, Molecular mechanisms of antibiotic resistance revisited, Nat. Rev. Microbiol. 21 (2023) 280–295.

[9] M. Miethke, M. Pieroni, T. Weber, M. Brönstrup, P. Hammann, L. Halby, P. B. Arimondo, P. Glaser, B. Aigle, H.B. Bode, Towards the sustainable discovery and development of new antibiotics, Nat. Rev. Chem 5 (2021) 726–749.

[10] N. Ayoub, A. Gedeon, H. Munier-Lehmann, A journey into the regulatory secrets of the *de novo* purine nucleotide biosynthesis, Front. Pharmacol. 15 (2024) 1329011.

[11] G.D. Cuny, C. Suebsuwong, S.S. Ray, Inosine-5'-monophosphate dehydrogenase (IMPDH) inhibitors: a patent and scientific literature review (2002-2016), Expert Opin. Ther. Pat. 27 (2017) 677–690.

[12] Y. Zhang, M. Morar, S.E. Ealick, Structural biology of the purine biosynthetic pathway, Cell. Mol. Life Sci. 65 (2008) 3699–3724.

[13] M.D. Sintchak, E. Nimmesgern, The structure of inosine 5′-monophosphate dehydrogenase and the design of novel inhibitors, Immunopharmacology 47 (2000) 163–184.

[14] R. Naffouje, P. Grover, H. Yu, A. Sendilnathan, K. Wolfe, N. Majd, E.P. Smith, K. Takeuchi, T. Senda, S. Kofuji, Anti-tumor potential of IMP dehydrogenase inhibitors: a century-long story, Cancers 11 (2019) 1346.

[15] R. Bentley, Mycophenolic acid: a one hundred year odyssey from antibiotic to immunosuppressant, Chem. Rev. 100 (2000) 3801–3826.

[16] J.E.S. Kitchin, M.K. Pomeranz, G. Pak, K. Washenik, J.L. Shupack, Rediscovering mycophenolic acid: a review of its mechanism, side effects, and potential uses, J. Am. Acad. Dermatol. 37 (1997) 445–449.

[17] L. Hedstrom, G. Liechti, J. B Goldberg, D. R Gollapalli, The antibiotic potential of prokaryotic IMP dehydrogenase inhibitors, Curr. Med. Chem. 18 (2011) 1909–1918.

[18] C.P. Shah, P.S. Kharkar, Inosine 5′-monophosphate dehydrogenase inhibitors as antimicrobial agents: recent progress and future perspectives, Future Med. Chem. 7 (2015) 1415–1429.

[19] R.M. Buey, D. Fernández-Justel, A. Jiménez, J.L. Revuelta, The gateway to guanine nucleotides: allosteric regulation of IMP dehydrogenases, Prot. Sci. 31 (2022) e4399.

[20] M. Makowska-Grzyska, Y. Kim, N. Maltseva, J. Osipiuk, M. Gu, M. Zhang, K. Mandapati, D.R. Gollapalli, S.K. Gorla, L. Hedstrom, A novel cofactor-binding mode in bacterial IMP dehydrogenases explains inhibitor selectivity, J. Biol. Chem. 290 (2015) 5893–5911.

[21] S.K. Gorla, M. Kavitha, M. Zhang, X. Liu, L. Sharling, D.R. Gollapalli, B. Striepen, L. Hedstrom, G.D. Cuny, Selective and potent urea inhibitors of *Cryptosporidium parvum* inosine 5′-monophosphate dehydrogenase, J. Med. Chem. 55 (2012) 7759–7771.

[22] K. Mandapati, S.K. Gorla, A.L. House, E.S. McKenney, M. Zhang, S.N. Rao, D. R. Gollapalli, B.J. Mann, J.B. Goldberg, G.D. Cuny, Repurposing cryptosporidium inosine 5′-monophosphate dehydrogenase inhibitors as potential antibacterial agents, ACS Med. Chem. Lett. 5 (2014) 846–850.

[23] B.J. Newhouse, J.D. Hansen, J. Grina, M. Welch, G. Topalov, N. Littman, M. Callejo, M. Martinson, S. Galbraith, E.R. Laird, Non-oxime pyrazole based inhibitors of B-Raf kinase, Bioorg. Med. Chem. Lett. 21 (2011) 3488–3492.

[24] S.H. Jung, K. Choi, A.N. Pae, J.K. Lee, H. Choo, G. Keum, Y.S. Cho, S.-J. Min, Facile diverted synthesis of pyrrolidinyl triazoles using organotrifluoroborate: discovery of potential mPTP blockers, Org. Biomol. Chem. 12 (2014) 9674–9682.

[25] A. Dyckman, W.J. Pitts, M. Belema, P. Gill, J. Kempson, Y. Qiu, C. Quesnelle, S. H. Spergel, F.C. Zusi, Imidazo-fused oxazolo [4, 5-b] pyridine and imidazo-fused thiazolo [4, 5-b] pyridine based tricyclic compounds and pharmaceutical compositions comprising same, US Patent US20050101626A1 (2008).

[26] N. Kudo, M. Perseghini, G.C. Fu, A versatile method for Suzuki cross-coupling reactions of nitrogen heterocycles, Angew. Chem. Int. Ed. 45 (2006) 1282–1284.

[27] K. Brunner, S. Maric, R.S. Reshma, H. Almqvist, B. Seashore-Ludlow, A.-L. Gustavsson, Ö. Poyraz, P. Yogeeswari, T. Lundbäck, M. Vallin, D. Sriram, R. Schnell, G. Schneider, Inhibitors of the cysteine synthase CysM with antibacterial potency against dormant *Mycobacterium tuberculosis*, J. Med. Chem. 59 (2016) 6848–6859.

[28] J.M. Khurana, A. Sehgal, An efficient and convenient procedure for ester hydrolysis, Org. Prep. Proced. Int. 26 (1994) 580–583.

[29] X.-G. Bai, D.-K. Yu, J.-X. Wang, H. Zhang, H.-W. He, R.-G. Shao, X.-M. Li, Y.-C. Wang, Design, synthesis and anticancer activity of 1-acyl-3-amino-1,4,5,6-tetrahydropyrrolo[3,4-c]pyrazole derivatives, Bioorg. Med. Chem. Lett. 22 (2012) 6947–6951.

[30] C.H.A. Lee, H.K.M. Nagaraj, A.D. William, M. Williams, Z. Xiong, Triazine compounds as kinase inhibitors, World Patent WO2009093981A1 (2009).

[31] S.J. Wood, T.M. Kuzel, S.H. Shafikhani, *Pseudomonas aeruginosa*: infections, animal modeling, and therapeutics, Cells 12 (2023) 199.

[32] G. Labesse, T. Alexandre, L. Vaupré, I. Salard-Arnaud, J.L.K. Him, B. Raynal, P. Bron, H. Munier-Lehmann, MgATP regulates allostery and fiber formation in IMPDHs, Structure 21 (2013) 975–985.

[33] T. Alexandre, A. Lupan, O. Helynck, S. Vichier-Guerre, L. Dugué, M. Gelin, A. Haouz, G. Labesse, H. Munier-Lehmann, First-in-class allosteric inhibitors of bacterial IMPDHs, Eur. J. Med. Chem. 167 (2019) 124–132.

[34] S.K. Gorla, N.N. McNair, G. Yang, S. Gao, M. Hu, V.R. Jala, B. Haribabu, B. Striepen, G.D. Cuny, J.R. Mead, L. Hedstrom, Validation of IMP dehydrogenase inhibitors in a mouse model of cryptosporidiosis, Antimicrob. Agents Chemother. 58 (2014) 1603–1614.

[35] Y. Kim, M. Makowska-Grzyska, S.K. Gorla, D.R. Gollapalli, G.D. Cuny, A. Joachimiak, L. Hedstrom, Structure of Cryptosporidium IMP dehydrogenase bound to an inhibitor with *in vivo* antiparasitic activity, Acta Crystallogr. F Struct. Biol. Commun. 71 (2015) 531–538.

[36] O. Tenaillon, D. Skurnik, B. Picard, E. Denamur, The population genetics of commensal *Escherichia coli*, Nat. Rev. Microbiol. 8 (2010) 207–217.

[37] S. Makvana, L.R. Krilov, *Escherichia coli* infections, Pediatr. Rev. 36 (2015) 167–170.

[38] S.Y. Tong, J.S. Davis, E. Eichenberger, T.L. Holland, V.G. Fowler Jr., *Staphylococcus aureus* infections: epidemiology, pathophysiology, clinical manifestations, and management, Clin. Microbiol. Rev. 28 (2015) 603–661.

[39] P. Nandhini, P. Kumar, S. Mickymaray, A.S. Alothaim, J. Somasundaram, M. Rajan, Recent developments in methicillin-resistant *Staphylococcus aureus* (MRSA) treatment: a review, Antibiotics 11 (2022) 606.

[40] World Health Organisation, WHO Priority Pathogens List for R&D of New Antibiotics, 2024.

[41] A. Gedeon, N. Ayoub, S. Brûlé, B. Raynal, G. Karimova, M. Gelin, A. Mechaly, A. Haouz, G. Labesse, H. Munier-Lehmann, Insight into the role of the Bateman domain at the molecular and physiological levels through engineered IMP dehydrogenases, Prot. Sci. 32 (2023) e4703.

[42] T. Alexandre, B. Rayna, H. Munier-Lehmann, Two classes of bacterial IMPDHs according to their quaternary structures and catalytic properties, PLoS One 10 (2015) e0116578.
[43] L. Hedstrom, IMP dehydrogenase: structure, mechanism, and inhibition, Chem. Rev. 109 (2009) 2903–2928.
[44] M. Nagai, Y. Natsumeda, G. Weber, Proliferation-linked regulation of type II IMP dehydrogenase gene in human normal lymphocytes and HL-60 leukemic cells, Cancer Res. 52 (1992) 258–261.
[45] H. Munier-Lehmann, A. Chaffotte, S. Pochet, G. Labesse, Thymidylate kinase of Mycobacterium tuberculosis: a chimera sharing properties common to eukaryotic and bacterial enzymes, Prot. Sci. 10 (2001) 1195–1205.
[46] B.Y. Feng, B.K. Shoichet, A detergent-based assay for the detection of promiscuous inhibitors, Nat. Protoc. 1 (2006) 550–553.
[47] F. Sievers, A. Wilm, D. Dineen, T.J. Gibson, K. Karplus, W. Li, R. Lopez, H. McWilliam, M. Remmert, J. Söding, J.D. Thompson, D.G. Higgins, Fast, scalable generation of high-quality protein multiple sequence alignments using Clustal Omega, Mol. Syst. Biol. 7 (2011) 539.
[48] X. Robert, P. Gouet, Deciphering key features in protein structures with the new ENDscript server, Nucleic Acids Res. 42 (2014) W320–W324.
[49] M.S. Alqahtani, M. Kazi, M.A. Alsenaidy, M.Z. Ahmad, Advances in oral drug delivery, Front. Pharmacol. 19 (2021) 618411.
[50] K. McCarthy, M. Minyon Avent, Oral or intravenous antibiotics? Aust. Prescr. 43 (2020) 45–48.
[51] V. Meunier, M. Bourrié, Y. Berger, G. Fabre, The human intestinal epithelial cell line Caco-2; pharmacological and pharmacokinetic applications, Cell Biol. Toxicol. 11 (1995) 187–194.
[52] S.K. Gorla, M. Kavitha, M. Zhang, J.E. Chin, X. Liu, B. Striepen, M. Makowska-Grzyska, Y. Kim, A. Joachimiak, L. Hedstrom, G.D. Cuny, Optimization of benzoxazole-based inhibitors of *Cryptosporidium parvum* inosine 5′-monophosphate dehydrogenase, J. Med. Chem. 56 (2013) 4028–4043.
[53] C. Blondin, L. Serina, L. Wiesmüller, A.M. Gilles, O. Bârzu, Improved spectrophotometric assay of nucleoside monophosphate kinase activity using the pyruvate kinase/lactate dehydrogenase coupling system, Anal. Biochem. 220 (1994) 219–221.
[54] L. Dubois, N. Pietrancosta, A. Cabaye, I. Fanget, C. Debacker, P.-A. Gilormini, P. M. Dansette, J. Dairou, C. Biot, R. Froissart, A. Goupil-Lamy, H.-O. Bertrand, F. C. Acher, I. McCort-Tranchepain, B. Gasnier, C. Anne, Amino acids bearing aromatic or heteroaromatic substituents as a new class of ligands for the lysosomal sialic acid transporter sialin, J. Med. Chem. 63 (2020) 8231–8249.
[55] O. Poirel, L.E. Mamer, M.A. Herman, M. Arnulf-Kempcke, M. Kervern, B. Potier, S. Miot, J. Wang, F.-C. Favre-Besse, I. Brabet, Y. Laras, H.-O. Bertrand, F. Acher, J.-P. Pin, J.-L. Puel, B. Giros, J. Epelbaum, C. Rosenmund, P. Dutar, S. Daumas, S. El Mestikawy, N. Pietrancosta, LSP5-2157 a new inhibitor of vesicular glutamate transporters, Neuropharmacology 164 (2020) 107902.
[56] J.D. Thompson, D.G. Higgins, T.J. Gibson, W. Clustal, Improving the sensitivity of progressive multiple sequence alignment through sequence weighting, position-specific gap penalties and weight matrix choice, Nucleic Acids Res. 22 (1994) 4673–4680.
[57] G. Wu, D.H. Robertson, C.L. Brooks, M. Vieth, Detailed analysis of grid-based molecular docking: a case study of CDOCKER-A CHARMm-based MD docking algorithm, J. Comput. Chem. 24 (2003) 1549–1562.
[58] A. Krammer, P.D. Kirchhoff, X. Jiang, C.M. Venkatachalam, M. Waldman, LigScore: a novel scoring function for predicting binding affinities, J. Mol. Graph. Model. 23 (2005) 395–407.
[59] M.A. Blaskovich, J. Zuegg, A.G. Elliott, M.A. Cooper, Helping chemists discover new antibiotics, ACS Infect. Dis. 1 (2015) 285–287.